

University of Nevada, Reno

Assessing the Sensitivity of a Volcanic Aquifer-Spring System to Climate Change

A thesis submitted in partial fulfillment of the requirements for the degree of Master of Science

in Hydrogeology

by

Lauren K. Mancewicz

Dr. Scott Tyler/Thesis Advisor

December, 2018



THE GRADUATE SCHOOL

We recommend that the thesis
prepared under our supervision by

LAUREN MANCEWICZ

Entitled

Assessing The Sensitivity Of A Volcanic Aquifer-Spring System To Climate Change

be accepted in partial fulfillment of the
requirements for the degree of

MASTER OF SCIENCE

Dr. Scott Tyler, Advisor

Dr. Greg Pohll, Committee Member

Dr. Mike Dettinger, Graduate School Representative

David W. Zeh, Ph.D., Dean, Graduate School

December, 2018

Abstract

The Fall River Spring system, located in northeastern California, is home to some of the largest first order springs in the U.S., with an average discharge of 34m³/s, and are a valuable water resource economically and ecologically. The goal of this thesis is to assess the possibility that climate change (warming and transition from snow to rain) will impact system recharge and to enhance the conceptual understanding of the aquifer-spring system. Spring discharge sampling for isotopic analysis of $\delta^{18}\text{O}$ and δD supplements past work and provides insight to the location of the recharge area. Chlorofluorocarbon sampling indicates an apparent groundwater age of 33 – 46 years. Calibration of a steady state MODFLOW model suggests a bulk hydraulic conductivity on the order of 10^2 m/d. Output from the Basin Characterization Model for responding to a projection of climate change reveals a decrease in average groundwater recharge from 44.1 cm/yr to 39.0 cm/yr across the watershed from the historic to end of century time periods. This response reflects an overall decrease in precipitation, increase in the proportion of precipitation that becomes actual evapotranspiration and decrease in snowfall.

Acknowledgements

I would like to thank Dr. Scott Tyler for the opportunity to pursue this degree and for his guidance and support. I would also like to thank Dr. Greg Pohll and Dr. Mike Dettinger for their involvement and insight. Additionally, I am grateful for the contribution of many others who helped to make this work possible. Lee Davisson shared his expertise and knowledge of the site providing direction. Peter Stent extended hospitality and generously allowed access for field sampling. Chris Kratt, Chris Sladek, Shawn Wheelock, and Charlie Breithaupt provided much valued assistance with field work. Guidance from Dr. Simon Poulson on the geochemical portion of this work and from Dr. Craig Smith on building the Python code was much appreciated, as was input from Dr. Erick Burns regarding the conceptual model. Theresa O'Halloran, John Volk, and Spencer Whitman imparted insightful conversation and encouragement. I would also like to thank and acknowledge my funding sources: UNR Graduate Program of Hydrologic Sciences, US Forest Service and UNR Graduate Student Association.

Table of Contents

Abstract.....	i
Acknowledgements.....	ii
Ch1 - Introduction.....	1
Background and Technical Need	3
Current Knowledge Base.....	4
Climate Change	6
Research Approach Description.....	8
References	9
Ch 2 – Geochemical Sampling.....	12
Introduction	12
Methods.....	16
Results and Discussion	18
Conclusions and Future Work.....	26
References	27
Ch 3 – Groundwater Model	30
Introduction	30
Methods.....	33
Results and Discussion	37
Conclusions and Future Work.....	44
References	45
Ch 4 – Basin Characterization Model Analysis.....	45
Introduction	47
Methods.....	49
Results and Discussion	53
BCM Output and Observation Data	53
Historical Scenario	55
GFDL A2.....	58
Conclusions and Future Work.....	68
References	69
Ch 5 – Conclusions and Future Work.....	71

Ch1 - Introduction

The Fall River Springs (FRS), located in Northern California (Figure 1.1), are some of the largest first order springs in the United States with an average cumulative discharge of $34\text{m}^3/\text{s}$ (Davisson & Rose, 2014). The Fall River Spring system is a valuable water resource for California's agriculture and hydropower industries, as well as ecologically. The water from the

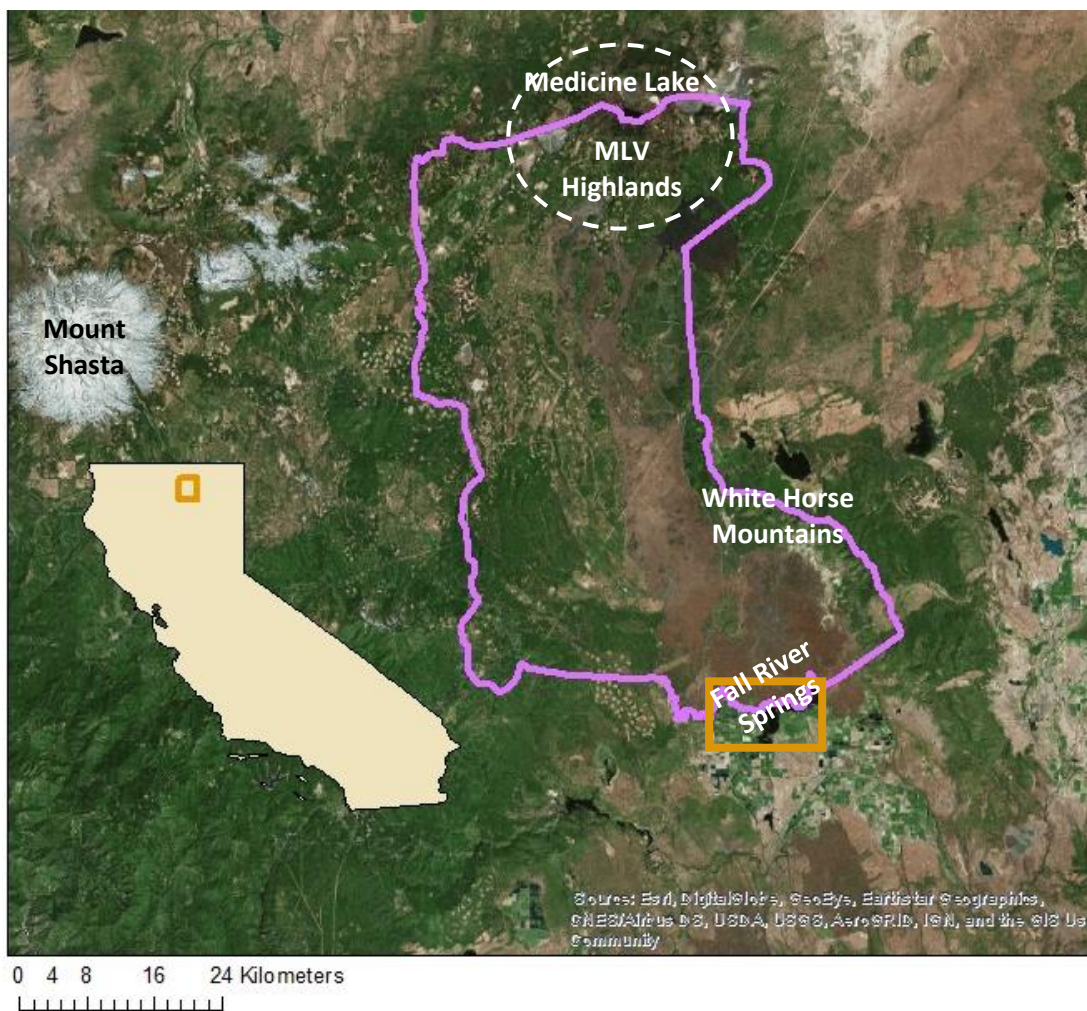


Figure 1.1: Site location. Outlined in purple is area used for the groundwater model domain and represents the site boundary. The white dashed line indicates the Medicine Lake Volcanic Highlands (MLVH) area. Medicine Lake is located near the center of the Highlands area. The Fall River Springs (FRS) discharge approximately 50 km south and downgradient of MLV Highlands. The orange inset is shown in Figure 1.2



Figure 1.2: Fall River Springs location of previously sampled springs by Davisson and Rose (2014) and is the inset of the orange outline in Figure 1.1.

Fall River Springs, and nearby hydrologically similar springs provide half the storage capacity of the Shasta Reservoir (Davisson and Rose, 1997). Flow from these springs also supply 10-15% of power generation for California. Furthermore, the cool nutrient rich discharge from the Fall River Spring provides habitat for threatened and endangered species (Davisson and Rose, 1997).

The volcanic aquifer that supplies water to the springs is thought to be comprised of the Giant Crater Lava flow, a basaltic flow that originated from Medicine Lake Volcano, a large shield volcano ~50 km north of FRS (Donnelly-Nolan et al., 1991). Due to the high permeability of the volcanic rock, it is estimated that up to 75% of the precipitation that falls on the upper parts of the watershed becomes recharge. Similarly, there are very limited surface water features throughout the site area. The combination of high permeability and infiltration, as well as the high discharge volumes of the springs, makes this site particularly hydrologically interesting.

Currently, the major recharge areas are dominated by winter snow (Davisson and Rose, 2014).

As temperatures rise, there is concern as to how this valuable freshwater source will be impacted. Therefore, the main research question addressed by this project is:

How does a change in temperature, and consequently a shift in precipitation from snow to rain, affect recharge at the Medicine Lake Highlands and on what timescale does this effect impact the FRS?

Thus, the goal of this research is to assess the potential for climate change (warming leading to increased evapotranspiration, and transition from snow to rain) to impact volcanic rock aquifer recharge. As a second goal, we seek to enhance the current conceptual understanding of the aquifer-spring system which has to date been generally poorly studied. Addressing these questions poses some interesting challenges in that limited in situ data exists and records are either not continuous or short term. Similarly, while monitoring of spring discharge is ongoing, these were only put in place over the last couple of years. Due to these challenges, care must be taken to develop an approach that is appropriate and takes into consideration these limitations. The findings from this project seek to enhance the current understanding of the system and provide an initial look at the impact of climate change of this valuable source of freshwater, while setting the stage for future work.

Background and Technical Need

Specifically, this work is motivated by the need to compile and utilize past and recent work to develop a more complete conceptual model, creating a foundation for future work on the Medicine Lake Volcanic Highlands Aquifer and FRS system. Additionally, this project is

motivated from work relating to the impact of increasing temperature on snow dominated areas due to climate change and the concern of how such an impact will affect recharge for the Medicine Lake Volcano Highlands Aquifer (MLVHA).

Current Knowledge Base

The Medicine Lake Volcano (MLV) is a half million-year-old shield volcano and is the largest by volume in the Cascades arc (Donnelly-Nolan, 2010). The caldera is at an elevation of 2440m and several cinder cones lie along its flanks (Donnelly-Nolan, 2010). MLV has erupted at least nine times in the past 5200 years, making it the second most frequently eruptive volcano of the Cascades. The lavas from these eruptions range from basalt through rhyolite and cover an area of 2000 km² (Donnelly-Nolan, 2010). One particular lava flow of hydrologic significance is the Giant Crater lava field. The Giant Crater eruption occurred approximately 10,500 years ago and produced 4.4 km³ of lava over a period of ten years (Donnelly-Nolan et al., 1991). Six chemically different lavas make up the lava field and each layer ranges in estimated thickness from 5 to 30 m (Donnelly-Nolan et al., 1991). The Giant Crater eruption occurred on the south west flank of MLV and stretches 45km to the south (Donnelly-Nolan et al., 1991). The Fall River Springs discharge from a 16 km wide section at terminus of the lava flow (Davisson and Rose, 2014). Discharge from the springs fluctuates on a 14 - 16 year cycle that appears to mirror trends in precipitation (Freeman, 2001) with an average discharge of 34 m³/s (M. Lee Davisson & Rose, 2014). Approximately one third of all discharge originates from the westernmost portion of the discharge zone (FRS-1 through FRS-5 in Figure 1.2) (M. Lee Davisson & Rose, 2014).

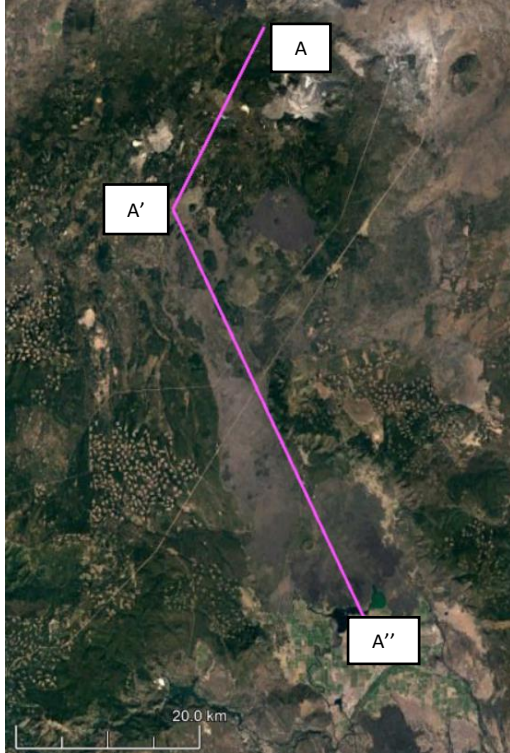


Figure 1.3: Site map showing transect that corresponds with Figure 4.

Also of note is the presence of a shallow geothermal reservoir at MLV at 1500 – 1100 m below the surface (Cumming and Mackie, 2007). The reservoir appears to be tightly sealed from the surface due to the lack of surface expression and the presence of an overlying low permeability layer. This layer is likely the result of hydrothermal alteration and is evident in geophysical surveys performed for geothermal exploration (Burns et al., 2017). Additionally, a significant increase in geothermal gradient indicates the presence of this impermeable cap (*Information Sheet Order No. R5-2006, 2006; Woodward, 2006*).

The cap formation could provide a localized bottom boundary for groundwater flow near MLV (C in Figures 1.3 and 1.4).

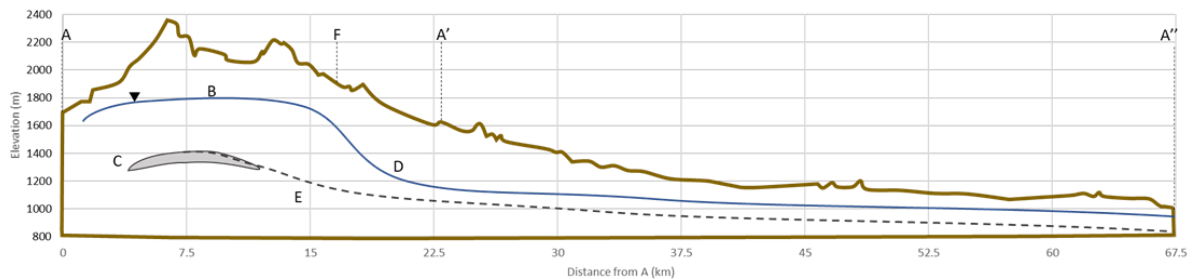


Figure 1.4: Cross section of transect from Figure 1.3 above showing the surface elevation and points as described. Point A'': Location of FRS. Point B: Approximate location of water table from measurements (Iovenitti and Hill, 1997). Point C: Elevation of clay cap at 1400m elevation. Point D: Approximate location of water level; at a surface elevation of 1700m, water table is at 1200m (Iovenitti and Hill, 1997). Point E: Dashed line represents unknown bottom of the aquifer. Point F: Elevation of Paynes Springs for reference (actual location of Paynes Springs is east of the transect).

The MLV Highlands are a significant source of recharge for the MLVHA. Analysis of $\delta^{18}\text{O}$ and δD from FRS and surrounding areas indicate that the discharge from the FRS has an isotopic composition similar to the groundwater on beneath MLV and is distinctly isotopically different from groundwater in the Klamath Valley, an area north of Medicine Lake originally believed to be a possible area of recharge (Davisson and Rose, 2014). Estimates indicate that 50 – 75% of precipitation falling on the MLV Highlands area becomes recharge, with average precipitation of 101 cm/yr at MLV (Davisson and Rose, 2014). Tritium age dating was also performed (Davisson and Rose, 2014). In completing the age dating analysis, certain samples were found to be enriched in helium, likely from magmatic sources. A linear correction was made to account for the additional helium resulting in an average groundwater age estimate of 20 years. However, analysis at some of the spring locations resulted in negative ages and further age dating analysis is needed (Davisson and Rose, 2014).

Climate Change

Currently the primary source of recharge for MLVHA is snowmelt (Davisson and Rose, 2014).

With increasing temperatures, multiple studies have found a decline in snow dominated precipitation across the western US (Freeman, 2012; Knowles et al., 2006; Lute et al., 2015; Lynn, 2015; Markovich et al., 2016; Safeeq et al., 2016). Modeled scenarios suggest that these changes will continue into the future (Dettinger et al., 2015). In one study, an increase in temperature by 1 degree C resulted in decrease in snow to precipitation proportion by 10-15% in the Northern Sierra, Klamath Mountains and western Cascades (Safeeq et al., 2016). This is further illustrated in Figure 1.5 with data from (Klos et al., 2014). These datasets provide a comparison of historical to projected climate change for both precipitation types in order

observe any transitions over time from one type to another. Historic (1979 – 2012) and modeled (2035 – 2065) mid-winter (December through January) wet day averages were determined using the multi-model means of downscaled data from 20 CMIP5 models for an emissions scenario of RCP 8.5 at 4km resolution. Figure 1.5 provides a stark contrast between the historic and future scenarios. While work by Klos et al. (2014) may be an overestimate of the shift in precipitation type (Harpold et al., 2017), the comparison of the scenarios in Figure 4 still raises concern and

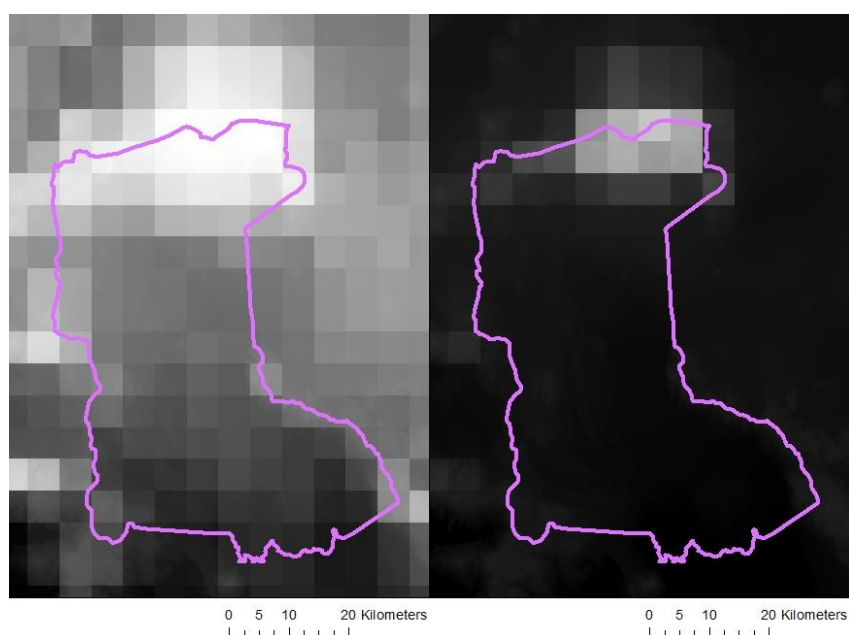


Figure 1.5: Probability of precipitation as snow from data by Klos et al. (2014). The right image shows average historical scenario and the left an averaged modeled future scenario. Outlined in purple is the groundwater model domain.

warrants additional investigation.

A shift in precipitation type can have implications for recharge, specifically with the increase in rain/snow ratio contributing to a decrease in recharge (Meixner et al., 2016; Portge, 2015).

Furthermore, the shift from snow to rain can impact the temperature of spring discharge.

Analysis from Burns et al. revealed a 1.5 degree C increase in temperature and 3.0 degree C increase in recharge temperature by mid-century at MLV would increase FRS discharge temperature by 1.75 degrees C with most of the change occurring in the first 60 years (Burns et al., 2017).

Research Approach Description

In order to address the research question above, the project has been split into three sections as seen in Figure 1.6; spring sampling, groundwater modeling, and Basin Characterization Model (BCM) analysis. Spring discharge sampling and groundwater flow modeling were done to improve the conceptual understanding of the system. Specifically, stable isotope analysis provides insight into recharge areas. From this analysis, the recharge elevation can be determined and used to calculate the recharge temperature from the ratio of dissolved nitrogen and argon ratio. The resulting recharge temperature was then used to calculate the apparent groundwater age from chlorofluorocarbon (CFC) sampling. The apparent age provides an idea

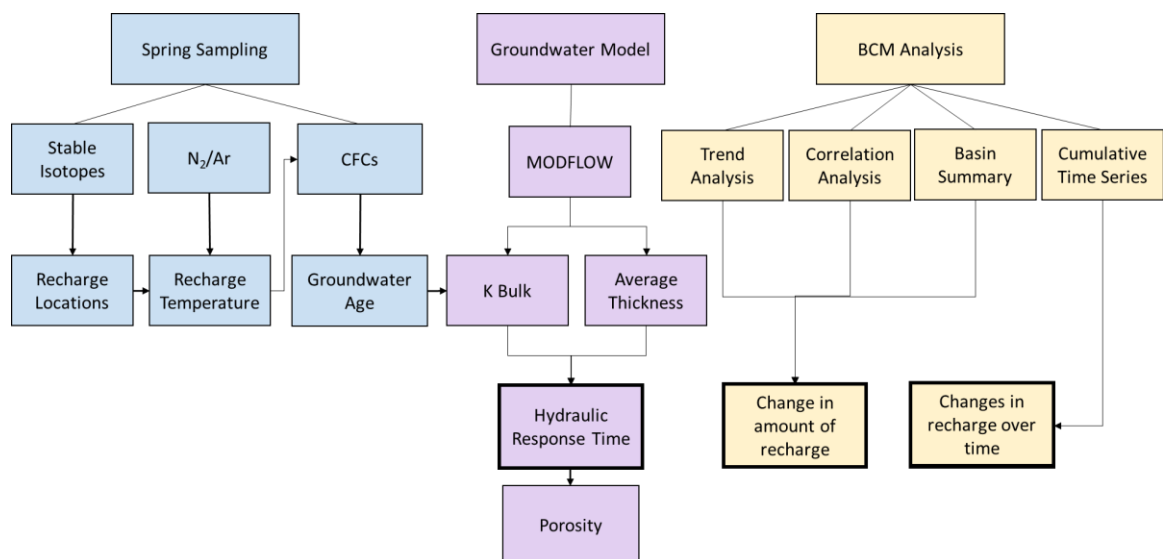


Figure 1.6: Outline of research approach.

on the timespan for which the system functions and was used in calculations to estimate hydraulic properties as a starting place for calibration of a groundwater flow model.

The groundwater model was calibrated based on limited hydrologic and geologic data and used to estimate a bulk hydraulic conductivity and the average thickness of the aquifer. Both of these properties were used in calculating the hydraulic response time; the time it takes for a change in input to affect the FRS. The hydraulic response time can also be used to calibrate the effective bulk porosity. This provides insight into the timescales over which changes to spring discharge may occur, as well as enhancing the overall understanding of the system.

Finally, output from an existing basin scale surface-hydrology model (BCM) was then used to assess aquifer recharge under a future climate condition. Trend and correlation analysis provides insight to possible shifts in relative amounts of recharge and associated climate variables. Examining cumulative yearly recharge elucidates the timing of recharge and related climate variables throughout the year. Each of these sections are discussed in detail in the following chapters.

References

Burns, E. R., Zhu, Y., Zhan, H., Manga, M., Williams, C. F., Ingebritsen, S. E., & Bunham, J. B. (2017). Thermal effect of climate change on groundwater-fed ecosystems. *Water Resources Research*, 3341–3351. <https://doi.org/10.1002/2016WR020007>.Received

Cumming, W., & Mackie, R. (2007). MT Survey for Resource Assessment and Environmental Mitigation at the Glass Mountain KGRA. Energy Research and Development Division Final Project Report.

- Davisson, M. L., & Rose, T. P. (1997). Comparative Isotope Hydrology Study of Groundwater in the Three Cascade Volcanoes of Northern California. Livermore.
- Davisson, M. L., & Rose, T. P. (2014). Recharge and Flow in the Medicine Lake Volcano – Fall River Springs Groundwater Basin, California. *Environmental Forensics*, 66–77. <https://doi.org/10.1080/15275922.2013.873097>
- Dettinger, M., Udall, B., & Georgakakos, A. (2015). Western water and climate change. *Ecological Applications*, 25(8), 2069–2093. <https://doi.org/10.1890/15-0938.1>
- Donnelly-Nolan, J. M. (2010). Geologic Map of Medicine Lake Volcano, Northern California. USGS.
- Donnelly-Nolan, J. M., Champion, D. E., Grove, T. L., Baker, M. B., Taggart, J. E., & Bruggman, P. E. (1991). The Giant Crater Lava Field: Geology and geochemistry of a compositionally zoned, high-alumina basalt to basaltic andesite eruption at Medicine Lake Volcano, California. *Journal of Geophysical Research: Solid Earth*, 96(B13), 21843–21863. <https://doi.org/10.1029/91JB01901>
- Freeman, G. J. (2001). The Impacts of Current and Past Climate on Pacific Gas & Electric 's 2001 Hydroelectric Outlook (pp. 21–38).
- Freeman, G. J. (2012). Analyzing the impact of climate change on monthly river flows in California's Sierra Nevada and southern Cascade mountain ranges. San Francisco.
- Harpold, A. A., Kaplan, M. L., Zion Klos, P., Link, T., McNamara, J. P., Rajagopal, S., ... Steele, C. M. (2017). Rain or snow: Hydrologic processes, observations, prediction, and research needs. *Hydrology and Earth System Sciences*, 21(1), 1–22. <https://doi.org/10.5194/hess-21-1-2017>
- Information Sheet Order No. R5-2006. (2006). Retrieved from https://www.waterboards.ca.gov/rwqcb5//board_decisions/tentative_orders/0605/calpine/calpine-info.pdf
- Klos, P. Z., Link, T. E., & Abatzoglou, J. T. (2014). Extent of the rain-snow transition zone in the western U.S. under historic and projected climate. *Geophysical Research Letters*, 41(13), 4560–4568. <https://doi.org/10.1002/2014GL060500>
- Knowles, N., Dettinger, M. D., & Cayan, D. R. (2006). Trends in Snowfall Versus Rainfall for the Western United States. *Journal of Climate*, 19, 4545–4559. Retrieved from <http://www.energy.ca.gov/2007publications/CEC-500-2007-032/CEC-500-2007-032.PDF>
- Lute, A. C., Abatzoglou, J. T., & Hegewisch, K. C. (2015). Projected changes in snowfall extremes and interannual variability of snowfall in the western United States. *Water Resources Research*, 51(2), 960–972. <https://doi.org/10.1002/2014WR016267>
- Lynn, E. (2015). California Climate Science and Data - For Water Resources Management.

Markovich, K. H., Maxwell, R. M., & Fogg, G. E. (2016). Hydrogeological response to climate change in alpine hillslopes. *Hydrological Processes*, 30(18), 3126–3138. <https://doi.org/10.1002/hyp.10851>

Meixner, T., Manning, A. H., Stonestrom, D. A., Allen, D. M., Ajami, H., Blasch, K. W., ... Walvoord, M. A. (2016). Implications of projected climate change for groundwater recharge in the western United States. *Journal of Hydrology*, 534, 124–138. <https://doi.org/10.1016/j.jhydrol.2015.12.027>

Portge, D. M. (2015). Comparison of the temporal development of vertical water movement in the unsaturated zone using the hydrological models Hydrus-1D and WaSiM Richards. *Technische Universität München*.

Safeeq, M., Shukla, S., Arismendi, I., Grant, G. E., Lewis, S. L., & Nolin, A. (2016). Influence of winter season climate variability on snow-precipitation ratio in the western United States. *International Journal of Climatology*, 36(9), 3175–3190. <https://doi.org/10.1002/joc.4545>

Woodward, P. (2006). Comments on placement of monitoring wells near geothermal production well No. 31-17, Telephone Flat geothermal exploration and development project, Siskiyou County, California. Redding, CA.

Ch 2 – Geochemical Sampling

Introduction

Geochemical analysis of spring discharge can provide useful information regarding groundwater recharge. In this study, spring discharge was sampled for stable isotopes, dissolved gases (nitrogen and argon) and chlorofluorocarbons (CFCs). An isotope refers to the varying forms of an atom containing a different number of neutrons. This results in different atomic masses between different isotopes of a certain element, and consequently relatively heavier and lighter versions of the element that behave differently in hydrologic processes. For example, lighter isotopes will preferentially evaporate compared to heavier isotopes, while condensation is preferentially enriched in heavier isotopes (Dansgaard, 1964; Mazor, 2004). Of interest for this project are the stable isotopes associated with water including ^1H (H), ^2H (deuterium, D), ^{18}O , and ^{16}O . Specifically, the ratios of $^{18}\text{O}/^{16}\text{O}$ and $^2\text{H}/^1\text{H}$ are analyzed here. These measurements are reported relative to a standard and in units of per mil (‰). This is written using delta notation for D and ^{18}O as follows:

$$\delta D \text{ ‰} = \frac{(D/H)_{\text{sample}} - (D/H)_{\text{standard}}}{(D/H)_{\text{standard}}} \times 1000 \quad \text{eq. 2-1}$$

$$\delta^{18}\text{O} \text{ ‰} = \frac{(^{18}\text{O}/^{16}\text{O})_{\text{sample}} - (^{18}\text{O}/^{16}\text{O})_{\text{standard}}}{(^{18}\text{O}/^{16}\text{O})_{\text{standard}}} \times 1000 \quad \text{eq. 2-2}$$

The relationship between ^{18}O and D on a global scale can be described by the Global Meteoric Water Line (GMWL). After plotting over 400 samples from surface water and precipitation the following linear relationship between $\delta^{18}\text{O}$ and δD was obtained:

$$\delta D = 8 \delta^{18}\text{O} + 10 \quad (\text{Craig, 1961}) \quad \text{eq. 2-3}$$

The GMWL serves as a reference line for interpreting sample results (Mazor, 2004). Samples taken from various areas that have similar isotopic compositions, also likely share a hydrologic

connection. Past isotope sampling in the study area includes groundwater and surface water sampling from FRS to the Klamath Basin, an area north of FRS (Mariner et al., 1998). Mariner et al. examined stable isotopes and general chemistry of water samples with the purpose of making the data publicly available for use in environmental impact reports relating to possible geothermal development around MLV (Mariner et al., 1998).

One significant finding from Mariner et al.'s study is that the discharge of the FRS does not appear to be hydrologically connected to the geothermal system at MLV Highlands.

Additionally, the chemistry of the FRS varies along the 16km discharge area, with slightly lower deuterium values in the middle region (Mariner et al., 1998). Palmer et al. collected isotope samples from groundwater and surface water in the upper Klamath Basin of the Cascade Range in order to elucidate groundwater recharge sources (Palmer et al., 2007). This data was used by Davisson and Rose, who compared the Klamath Basin data with that from FRS to evaluate whether this area north of MLV might be a source of recharge for the FRS. Water collected in the Klamath Basin, however, exhibited a characteristic evaporative trend while the FRS data plotted nearer to the GMWL (Davisson & Rose, 2014). Interpretation of isotopic data can provide valuable insight to recharge locations, and consequently recharge elevation, which is a necessary variable when determining recharge temperature.

A common method for determining recharge temperature uses the concentration of dissolved noble gasses (Aeschbach-Hertig et al., 1999; Ballentine & Hall, 1999; Böhlke & Krantz, 2003; Cey et al., 2009; M. Lee Davisson & Rose, 2014; Manning & Caine, 2007; Manning & Solomon, 2003;

Masbruch et al., 2012; Segal et al., 2014). Once water percolates downward and enters the aquifer, it is no longer in contact with the air and concentrations of gases in the water are relatively fixed. The concentration of gas that dissolves into the groundwater depends on the properties of the specific gas itself and the noble gas temperature (Weiss, 1970). This noble gas temperature is representative of the temperature of the recharge water. For any given temperature, a certain amount of N₂ and Ar exist at equilibrium. From this, a relationship between N₂ and Ar concentrations and temperature can be established. Therefore, by measuring the concentrations of N₂ and Ar, the temperature can be backed out.

Often the measured concentrations of dissolved gases are greater than the expected equilibrium concentrations with respect to atmospheric conditions. This is attributed to “excess air” that is trapped in bubbles as the water is percolating down towards the water table. While the exact mechanism for how air becomes entrapped in groundwater is still not well understood, in general bubbles that are carried below the water table experience increased hydrostatic pressure and eventually dissolve into the groundwater (Aeschbach et al., 2000; Cey et al., 2009; Heaton & Vogel, 1981). To correct for this, a back solving routine can be used to iteratively calculate the recharge temperature until the calculated amount of excess air indicated by the N₂ and Ar values are the same (Busenberg, 2012). Recharge temperatures derived from dissolved neon and argon concentrations, based off of similar theory, ranged from 5 to 10 degrees C (M. Lee Davisson & Rose, 2014). The recharge temperature is then used in calculating the apparent age of the spring water using CFC concentrations (Plummer et al., 2006).

CFCs are manmade compounds that were originally produced in the 1930s for industrial and refrigeration applications, that ultimately escaped into the atmosphere. CFCs were found to deplete ozone in the stratosphere and virtually all nations began limiting the use of CFCs starting in 1987. In the U.S., further production of CFCs was banned under the Clean Air Act in 1996. Since this time, the atmospheric concentrations have declined. While there are several different CFC compounds, those of hydrologic interest are CFC-11, CFC-12, and CFC-113 (Plummer & Busenberg, 2006). The concentrations of these compounds in the atmosphere have been directly measured or reconstructed over time. Similar to the dissolved noble gas analysis, it is assumed that a groundwater sample was in equilibrium with the air in the unsaturated zone at the time of recharge, which is also dependent on pressure and temperature. Once the downward percolating recharge water is within the aquifer and no longer in contact with the atmosphere, the concentration of CFCs is relatively fixed. A measured CFC concentration from a sample can then be matched to the date that corresponds with the known atmospheric CFC concentration (Plummer et al., 2006).

Groundwater ages at the FRS, based on using tritium as a tracer, ranges from 1 – 28 years (M. Lee Davisson & Rose, 2014). Tritium dating is based on both the concentration of tritium, as well as helium, which is the daughter product of tritium decay. Excess helium from magmatic environments, such as MLV, can impact the tritium ages because it is an additional source of helium. Thus, while past age dating has been performed, a different method may provide additional insight to the groundwater age of the spring discharge.

Methods

Spring water was sampled for analysis of stable isotopes, dissolved gases, and CFCs.

Interpretation of isotopic results from spring discharge sampling and comparison to past efforts helps to elucidate recharge processes for the MLVHA-FRS system. The elevation at which recharge occurs is required for the dissolved gas analysis. Therefore, there must be an understanding of the relative recharge location prior to calculating the recharge temperatures. The apparent age from CFC concentrations is dependent on this recharge temperature and was compared to previous age dating work using tritium in order to validate past efforts (Davisson & Rose, 2014; Szabo et al., 1996). A representative groundwater age from this analysis was used in calculating initial estimates of aquifer travel times for the groundwater model calibration discussed in Chapter 3.

Spring discharge was sampled at six different locations along the MLVH-FRS system (Figure 2.1 and 2.2). Locations were chosen based on sample locations in previous work so that comparisons could be made. This includes FRS-4, FRS-12, and RS-1 which are all located at the southern toe of the lava flow. Additionally, locations were chosen throughout the watershed in attempt to make a broader assessment of the system. These locations include Paynes Springs, located in the MLV Highlands area, and Wiley-1 and Wiley-2, both located in the eastern area of the site near the White Horse Mountains. Samples for determination of dissolved noble gasses, CFCs, and stable isotopes were collected at Paynes Springs, FRS-4, FRS-12 and RS-1. Stable isotopes were additionally sampled at Wiley 1 and Wiley 2. Dissolved noble gasses and CFCs

were not collected at Wiley 1 and Wiley 2 due to the presence of a spring box exposing the sample to atmospheric conditions and low discharge rates respectively.

Spring discharge was sampled following methods outlined by the USGS Groundwater Dating Lab (Busenberg et al., 2006; "CFC Bottle Sampling Method," 2018; "Dissolved Gas N₂ / Ar Sample Collection Procedure," 2018). A peristaltic pump with viton flexible tubing and refrigeration grade copper tubing was used at all locations to prevent contamination of the CFC samples. At Paynes Springs, however, instead of a pump the flow was sufficient to sample directly from the spring with the copper tubing. The copper tubing was placed directly into the spring discharge which occurred at a discrete location, with the exception of Wiley-1 and Wiley-2. At Wiley-1, a pipe with a valve was outfitted to a spring box located upgradient. The sample was collected from the outflow of this pipe. At Wiley-2, discharge occurs in a diffuse seep and a wellpoint was driven into the subsurface in attempt to collect the sample. However, as mentioned above, the flow rate was too low for proper sampling protocol to be followed and only stable isotope samples were collected after purging the well and allowing it to refill.

Field parameters, including temperature, electrical conductivity and pH, were measured and assessed for stabilization prior to sampling (Table 2.1). However, due to the low flowrate at Wiley-2, no field parameters were recorded at this location. The field parameter instruments were calibrated in the lab as well as on site prior to use. Stable isotopes were analyzed at the

University of Nevada, Reno. CFCs and dissolved gases samples were analyzed at the USGS Groundwater Dating Lab in Reston, VA.

The $\delta O\text{‰}$ and $\delta D\text{‰}$ values were plotted and compared to past isotope sampling over time and by location (Figures 2.3 – 2.6). A sensitivity analysis was conducted for the N_2/Ar recharge temperature data. Since only an approximate recharge area could be determined, largely based on the isotope data, the exact recharge elevation is not precisely known. Therefore, a range of elevations was tested to evaluate the impact of this uncertainty in recharge elevation on the resulting calculations of recharge temperatures and apparent ages.

Results and Discussion

Parameter stabilization results are shown in Table 2.1. Results from recent and past stable isotope sampling are shown in Figures 2.3 – 2.6. The Global Meteoric Water Line (GMWL) is also included for reference (Craig, 1961). Isotope samples taken from the FRS area are consistent with past isotope results collected in 1997 (Davisson & Rose, 2014; Mariner et al., 1998) and 1993 (Mariner et al., 1998) (Figure 2.3). The $\delta O\text{‰}$ and $\delta D\text{‰}$ values narrowly range from -13.8 to -13.2‰ and -103 to -93‰ respectively. This range among springs is relatively small overall, and especially when considering the changes that occur at each individual location. Therefore, the changes over time do not appear to be significant, as the mere effect of seasonality can

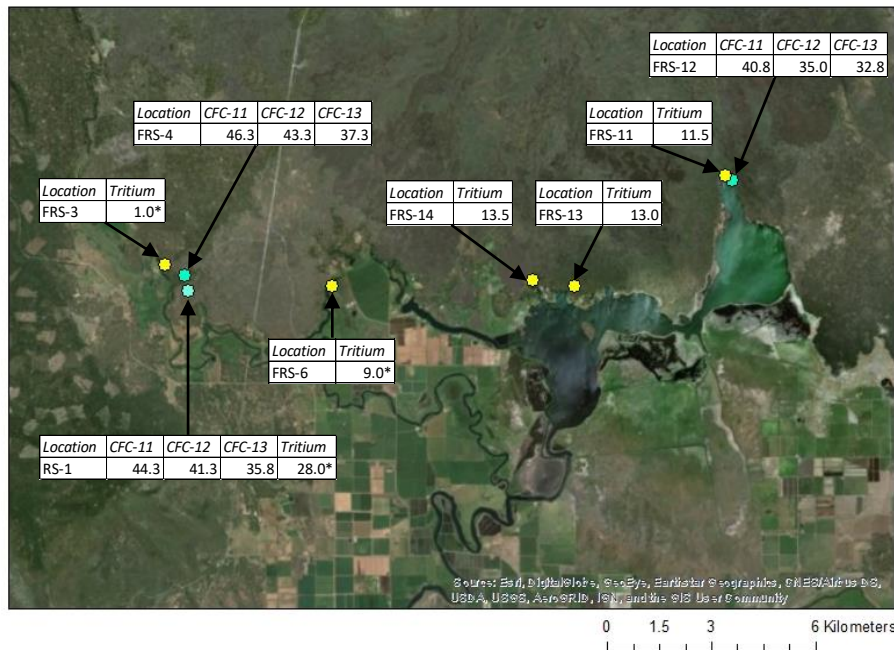


Figure 2.1 (left) and 2.2 (above): Sample locations and age dating data in years. Figure 2.2 is the inset of the purple region on Figure 2.1. Light blue markers indicate samples taken in fall 2017. Yellow markers indicate samples taken in 1997 by Davisson and Rose (2014). Tritium and CFC piston flow apparent ages are presented. For the tritium ages, the “*” indicates that the sample contained excess helium and a linear correction was applied. The 2017 samples (light blue markers) were additionally sampled for stable isotopes.

cause variation of 0.5 $\delta\text{O}\%$ /degree C (Gat et al., 2001). Additionally, results from Wiley-1 (-13.5 $\delta\text{O}\%$, -97 $\delta\text{D}\%$) and Wiley-2 (13.4 $\delta\text{O}\%$, -97 $\delta\text{D}\%$) are isotopically similar to FRS, implying that the White Horse Mountains could be a potential source of recharge. Springs sampled in the MLV Highlands area, which does not include Wiley-1 and Wiley-2, are also relatively consistent over time, with the exception of Paynes Springs (Figure 2.4) (Mariner et al., 1998). The earliest sample from Paynes Springs (July 1982) has an isotopic composition of -13.6 $\delta\text{O}\%$ and -105 $\delta\text{D}\%$, while recent measurements (September 2017) have values of -13.0 $\delta\text{O}\%$ and -93 $\delta\text{D}\%$.

Table 2.1: Field parameters for sample locations.

Location	Date	Field Parameter		
		Temperature (°C)	pH	Electrical Conductivity (μS)
Paynes Springs	9/9/2017	7.48	8.36	62
FRS-12	10/21/2017	12.89	8.86	168
FRS-4	10/22/2017	10.99	9.15	136
RS-1	10/22/2017	12.64	9.06	131
Wiley-1	9/9/2017	18.00	8.66	162
Wiley-2	9/25/2017	-	-	-

It was initially expected that the spring discharge at Paynes Springs would be similar in composition to the FRS samples, as Paynes Springs are located in the recharge area for the FRS. However, the recent values for Paynes Springs appear isotopically different compared to recent sampling at the FRS.

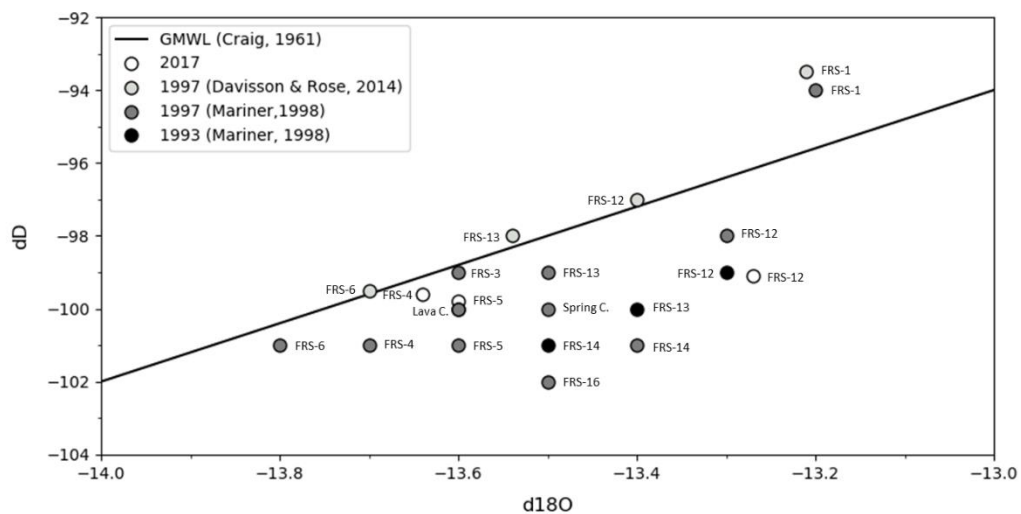


Figure 2.3: Stable isotope data for the FRS.

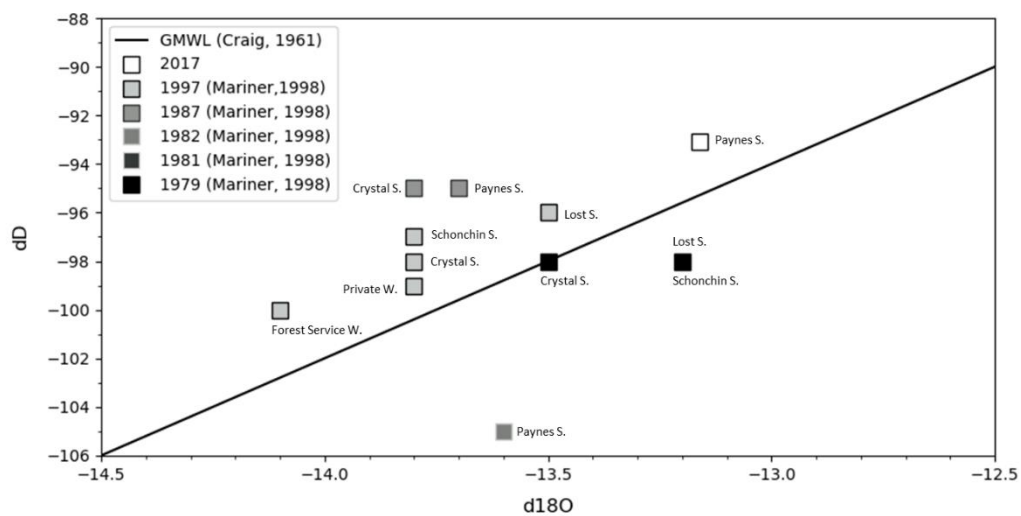


Figure 2.4: Stable isotope data for MLV area springs.

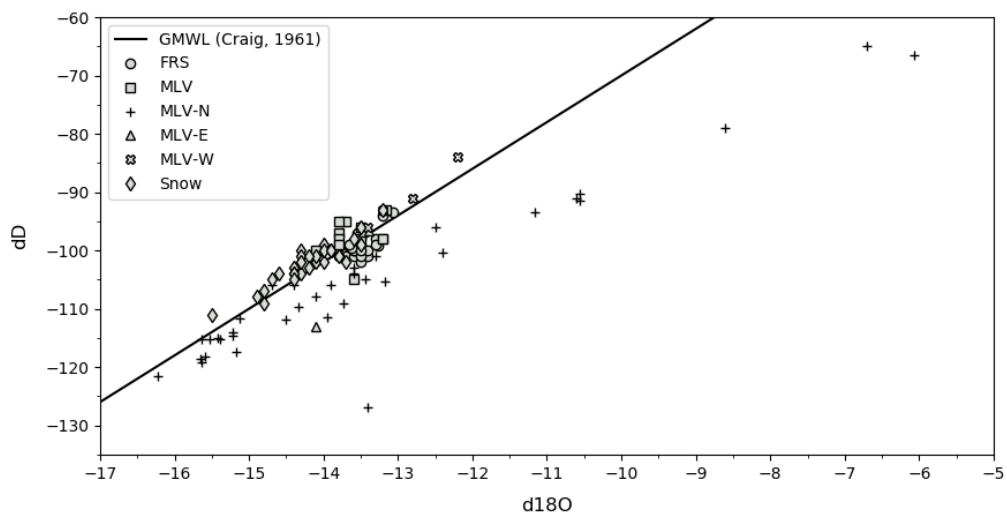


Figure 2.5: Total stable isotope data from FRS, MLV basin (MLV, MLV-E, and MLV-W, indicating within the caldera or on the flanks of MLV, east and west respectively) and the Klamath Basin area (MLV-N, north of MLV) (Davisson & Rose, 2014; Mariner et al., 1998; Palmer et al., 2007).

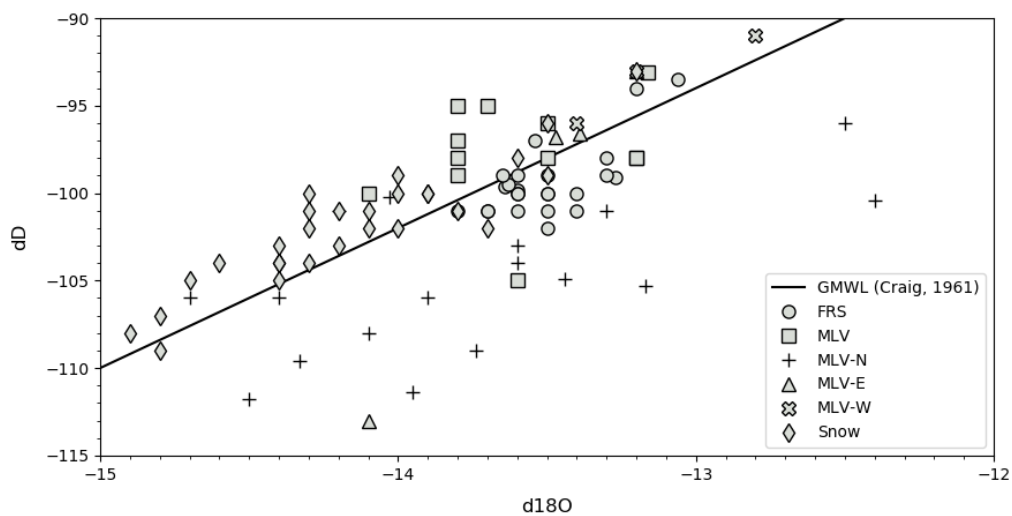


Figure 2.6: Total stable isotope data from FRS, MLV and the Klamath Basin area (Davisson & Rose, 2014; Mariner et al., 1998; Palmer et al., 2007).

When looking at the isotope data by location (Figures 2.5 and 2.6), the FRS samples appear isotopically similar to those from MLV, and are distinctly different from the Klamath Basin. The Klamath Basin is an area north of MLV and was originally believed to be a possible source of recharge for the FRS, as mentioned above. However, the samples from this area exhibit a characteristic evaporative signature that is likely a result of the extensive irrigation in the area, agreeing with and supporting past work (Davisson & Rose, 2014).

Table 2.2: Dissolved gas recharge temperature and excess air at different elevations.

Location	Elevation			
	2200 m		1400 m	
	Recharge Temperature (°C)	Excess Air (cc(STP)/L)	Recharge Temperature (°C)	Excess Air (cc(STP)/L)
Paynes Springs	2.3	3.2	5.9	3.0
FRS-12	6.8	1.0	10.7	0.8
FRS-4	5.1	1.1	8.8	0.9
RS-1	5.9	0.9	9.7	0.7

Results from N₂/Ar recharge temperatures are shown in Table 2.2. These values fall within the range of noble gas recharge temperature estimates of 5° – 10° C from past studies (M. Lee Davisson & Rose, 2014). Apparent ages from CFC sampling is shown in Figure 2.1 and 2.2. The CFC ages at FRS range from 33 – 46 years and at Paynes Springs the age is approximately 30 years. The recharge temperature at Paynes Springs for a recharge elevation of 2200m was 3.3° C with excess air of 3.1 cc(STP)/L while the recharge temperature at FRS ranges from 6.1° – 7.8° C with excess air of 0.8 – 1.0 cc(STP)/L. Of note, again, is the difference in Paynes Springs from FRS for both CFC ages and recharge temperature. Even though Paynes Springs is nearly 50km upgradient from FRS, the two springs unexpectedly have similar CFC apparent ages. Additionally, because Paynes Springs are located in the recharge source area for FRS, it would be

seem likely that the recharge temperature for both springs would be similar, however this is not the case.

The combination of isotopic signature, recharge temperature, and apparent age for Paynes Springs suggest that these springs likely differ hydrologically from FRS. One interpretation is that Paynes Springs are hydrologically connected to Medicine Lake. Medicine Lake has no natural surface outlet and is only drained by groundwater leakage. Thus, the lake is subject to evaporation. This is evident in the isotopic signature of samples taken from the lake and corresponds to the higher isotopic values in recent samples from Paynes Springs (Iovenitti & Hill, 1997). Furthermore, source water from the lake could cause the observed increase in groundwater ages at Paynes Springs due to increased residence time within Medicine Lake before becoming recharge for the springs. This is in comparison to FRS, where a majority of the recharge is from flow directly through the unsaturated zone. Overall, this hydrologic interpretation for Paynes Springs is supported by Iovenitti and Hill who note that the elevation of Paynes Springs is less than Medicine Lake, and also suggest that the source for Paynes Springs is likely within the caldera of MLV (Iovenitti & Hill, 1997).

A sensitivity analysis was performed on the N_2/Ar results to evaluate the impact of recharge location (elevation) on dissolved noble gas temperatures, and consequently the CFC ages. Recharge elevations from 2200m to 1600m were evaluated for each sample. The resulting recharge temperatures varied from $9.6^\circ - 5.5^\circ$ C for a recharge elevation of 2200m to $12.7^\circ -$

8.3° C at an elevation of 1600m. Despite this significant change in recharge temperature, the resulting CFC apparent ages varied only by -2 to + 1 years.

Also shown on Figures 2.1 and 2.2 are tritium apparent ages from Davisson & Rose (2014). CFC dating differs from past tritium dating by approximately 20 years. Tritium is considered to be a more conservative tracer compared to CFCs (Han et al., 2006). Relative agreement between CFC and tritium results provides greater confidence in age interpretation (Han et al., 2006). In one study, Szabo et al. noted the similarity between CFC and tritium ages and found no statistical difference between the two ages (Szabo et al., 1996). As previously mentioned, tritium age calculations for FRS were impacted by helium added from volcanic sources (Davisson & Rose, 2014). Additionally, since the CFC ages are older compared to the tritium ages, this discrepancy could possibly be influenced by the unsaturated zone lag time. For water tables deeper than 10m, the CFC concentration at the water table may not be representative of atmospheric conditions and instead are a function of transport rates through the unsaturated zone (Cook et al., 2006; Cook & Solomon, 1995). If this lag time is not taken into account, the apparent CFC age can be too large. The water table on the flanks of MLV caldera is noted as being very erratic spatially and over 90m below the ground surface (*Information Sheet Order No. R5-2006*, 2006). For comparison, lag times calculated in 2002 for a 30m and 40m deep water table are 12-15 years and 16 – 21 years respectively (Cook & Solomon, 1995). Thus, age estimates could be improved upon by modeling the unsaturated zone lag times for CFCs at MLV Highlands area. This currently proves difficult due to the lack of hydrologic data in this area. Also of note is that the CFC results are relatively consistent compared to the corrected tritium ages which vary from 1 – 29 years. While CFC age dating is subject to additional interpretation, these recent efforts

provide a useful comparison to past work and may represent a more definite groundwater age range.

Conclusions and Future Work

Results of stable isotope analysis of FRS discharge are similar to past work and show little change in the values over time. Samples at this location cluster around the GMWL similarly to analysis by Davisson and Rose and are isotopically different from samples in the Klamath Basin, an area previously believed to a possible recharge source for FRS (Davisson & Rose, 2014). The calculated recharge temperature from dissolved noble gases for FRS ranges from 5.1 to 6.8 degrees C. Apparent CFC ages range from 33 to 46 years and may be a more representative apparent groundwater age, indicating quick transport times compared to other hydrologic systems. An analysis of unsaturated zone thickness and modeling of CFC transport through this zone would provide additional insight to the apparent age of the groundwater discharge at FRS.

Isotopic and CFC apparent age from Paynes Springs suggest that these springs are hydrologically different from FRS. Stable isotopes at Paynes Springs slightly increase over time. The recharge temperature from noble gas sampling ranges from 6.1 – 7.8° C with the apparent age of 30 years. The combination of isotopic signature, and greater than expected apparent age suggest that Paynes Springs might be hydrologically connected to Medicine Lake. Isotopic profiling of Medicine Lake and further sampling of spring discharge could additionally elucidate the isotopic results at Paynes Springs and the hydrologic relationship between the two.

References

- Aeschbach-Hertig, W., Peeters, F., Beyerle, U., & Kipfer, R. (1999). Interpretation of dissolved atmospheric noble gases in natural waters. *Water Resources Research*, 35(9), 2779–2792.
- Aeschbach F; Beyerle, U; Kipfer, R, W. P. (2000). Paleotemperature reconstruction from noble gases in groundwater taking into account equilibration with entrapped air. *Nature*, 405(June), 1040–1044. <https://doi.org/10.1038/35016542>
- Ballentine, C. J., & Hall, C. M. (1999). Determining paleotemperature and other variables by using an error-weighted, nonlinear inversion of noble gas concentrations in water. *Geochimica et Cosmochimica Acta*, 63(16), 2315–2336. [https://doi.org/10.1016/S0016-7037\(99\)00131-3](https://doi.org/10.1016/S0016-7037(99)00131-3)
- Böhlke, K., & Krantz, D. E. (2003). *Isotope Geochemistry and Chronology of Offshore Ground Water Beneath Indian River Bay , Delaware*. Reston, Virginia.
- Busenberg, E. (2012). *N₂Ar*. U.S. Geological Survey.
- Busenberg, E., Plummer, L. N., Cook, P. G., Solomon, D. K., Han, L. F., Groning, M., & Oster, H. (2006). Sampling and analytical methods. In *Use of chlorofluorocarbons in hydrology* (pp. 199–220). Vienna: International Atomic Energy Agency.
- Cey, B. D., Hudson, G. B., Moran, J. E., & Scanlon, B. R. (2009). Evaluation of noble gas recharge temperatures in a shallow unconfined aquifer. *Ground Water*, 47(5), 646–659. <https://doi.org/10.1111/j.1745-6584.2009.00562.x>
- CFC Bottle Sampling Method. (2018). Retrieved May 1, 2017, from <https://water.usgs.gov/lab/chlorofluorocarbons/sampling/bottles/>
- Cook, P. G., Plummer, L. N., Solomon, D. K., Busenberg, E., & Han, L. F. (2006). Effects that can modify apparent CFC age. In *Use of chlorofluorocarbons in hydrology* (pp. 31–58). Vienna: International Atomic Energy Agency.
- Cook, P. G., & Solomon, D. K. (1995). Transport of Atmospheric Trace Gases to the Water Table: Implications for Groundwater Dating with Chlorofluorocarbons and Krypton 85. *Water Resources Research*, 31(2), 263–270. <https://doi.org/10.1029/94WR02232>
- Craig, H. (1961). Isotopic Variations in Meteoric Waters. *Science*, 133(3465), 1702–1703. Retrieved from <http://www.jstor.org/stable/1708089>
- Dansgaard, W. (1964). Stable isotopes in precipitation. *Tellus*, 16(4), 436–468. <https://doi.org/10.3402/tellusa.v16i4.8993>
- Davisson, M. L., & Rose, T. P. (2014). Recharge and Flow in the Medicine Lake Volcano – Fall River Springs Groundwater Basin , California. *Environmental Forensics*, 66–77. <https://doi.org/10.1080/15275922.2013.873097>
- Dissolved Gas N₂ / Ar Sample Collection Procedure. (2018). Retrieved May 1, 2018, from <https://water.usgs.gov/lab/dissolved-gas/sampling/>

- Gat, J. R., Mook, W. G., & Meijer, A. J. (2001). Environmental isotopes in the hydrological cycle, principles and applications. Volume II: Atmospheric water. IHP-V, Technical Document (Vol. 2). Retrieved from http://www.hydrology.nl/images/docs/ihp/Mook_II.pdf
- Han, L. F., Groning, M., Plummer, L. N., & Solomon, D. K. (2006). Comparison of the CFC technique with other techniques (^3H , $^3\text{H}/^3\text{He}$, ^{85}Kr). In Use of chlorofluorocarbons in hydrology (pp. 191–198). Vienna: International Atomic Energy Agency.
- Heaton, T. H. E., & Vogel, J. C. (1981). "Excess air" in groundwater. *Journal of Hydrology*, 50, 201–216.
- Information Sheet Order No. R5-2006. (2006). Retrieved from https://www.waterboards.ca.gov/rwqcb5//board_decisions/tentative_orders/0605/calpine/calpine-info.pdf
- Iovenitti, J. L., & Hill, D. G. (1997). Baseline hydrogeology evaluation report for Telephone Flat geothermal project Medicine Lake, California. Emeryville, CA. Retrieved from https://books.googleusercontent.com/books/content?req=AKW5Qad9SySHToSdN_BO07WJvgDJj7yUtasyPszA8B2oZdFhiY_PQ4q33I6DPvtVQrdLgv5CvzgDE9SsvpgKjWeM9Zxwlfmqb-xFYp8ANPDZE248QQ70u8Bltb63Bi6nbCiaVGRo2UzHVC8zu1AHwOdCeU4I9qXfjAM-3QSAH1_a5-NexKaYuFRF9L1_JDZx0dxW-zQ-d
- Manning, A. H., & Caine, J. S. (2007). Groundwater noble gas, age, and temperature signatures in an Alpine watershed: Valuable tools in conceptual model development. *Water Resources Research*, 43(4). <https://doi.org/10.1029/2006WR005349>
- Manning, A. H., & Solomon, D. K. (2003). Using noble gases to investigate mountain-front recharge. *Journal of Hydrology*, 275(3–4), 194–207. [https://doi.org/10.1016/S0022-1694\(03\)00043-X](https://doi.org/10.1016/S0022-1694(03)00043-X)
- Mariner, R. H., Evans, W. C., & Huebner, M. (1998). Preliminary chemical and isotopic data for waters from springs and wells on and near Medicine Lake Volcano, Cascade Range, northern California. Open-File Report 98-2. Menlo Park. Retrieved from <http://pubs.er.usgs.gov/publication/ofr982>
- Masbruch, M. D., Chapman, D. S., & Solomon, D. K. (2012). Air, ground, and groundwater recharge temperatures in an alpine setting, Brighton Basin, Utah. *Water Resources Research*, 48(10), 1–12. <https://doi.org/10.1029/2012WR012100>
- Mazor, E. (2004). *Chemical and Isotopic Groundwater Hydrology* (3rd ed.). New York: Marcel Dekker, Inc.
- Palmer, P. C., Gannett, M. W., & Hinkle, S. R. (2007). Isotopic characterization of three groundwater recharge sources and inferences for selected aquifers in the upper Klamath Basin of Oregon and California, USA. *Journal of Hydrology*, 336(1–2), 17–29. <https://doi.org/10.1016/j.jhydrol.2006.12.008>

- Plummer, L. N., & Busenberg, E. (2006). Chlorofluorocarbons in the atmosphere. In Use of chlorofluorocarbons in hydrology (pp. 9–16). Vienna: International Atomic Energy Agency. Retrieved from https://www-pub.iaea.org/MTCD/publications/PDF/Pub1238_web.pdf
- Plummer, L. N., Busenberg, E., & Cook, P. G. (2006). Principles of chlorofluorocarbon dating. In Use of chlorofluorocarbons in hydrology (pp. 17–29). Vienna: International Atomic Energy Agency.
- Segal, D. C., Moran, J. E., Visser, A., Singleton, M. J., & Esser, B. K. (2014). Seasonal variation of high elevation groundwater recharge as indicator of climate response. *Journal of Hydrology*, 519(PD), 3129–3141. <https://doi.org/10.1016/j.jhydrol.2014.10.051>
- Szabo, Z., Rice, D. E., Plummer, L. N., Busenberg, E., & Drenkard, S. (1996). Age dating of shallow groundwater with chlorofluorocarbons , tritium / helium 3 , and flow path analysis , southern New Jersey coastal plain. *Water Resources*, 32(4), 1023–1038.
- Weiss, R. F. (1970). The solubility of nitrogen, oxygen and argon in water and seawater. *Deep-Sea Research*, 17, 721–735.

Ch 3 – Groundwater Model

Introduction

Groundwater modeling is a valuable tool for elucidating aquifer properties. Through model calibration and model behavior, the conceptual understanding of a system can be enhanced. In these ways, the groundwater model can be used as a tool to evaluate a range of possible aquifer properties, rather than definitively estimate the specific aquifer properties at a certain location in settings where hydrologic and aquifer data are limited. This is the approach taken for the MLVHA-FRS system in order to develop a baseline groundwater model and contribute to the overall understanding.

Past modeling done on the system by Burns et al. focused on the potential impact of changing recharge temperature, as a response to changing precipitation type from snow to rain, on spring discharge temperature. Results showed that a 1.5 degree C increase in annual air temperature and resulting 3.0 degree C increase in recharge temperature by mid-century at MLV would increase FRS discharge temperature by 1.75 degrees C with most of the change occurring in the first 60 years (Burns et al., 2017). Past hydrologic work primarily focused on stable isotope sampling of groundwater and surface water in order to evaluate possible recharge areas (Davisson & Rose, 2014; Meinzer, 1927; Palmer et al., 2007). Historic spring discharge for the FRS were also recorded by Meinzer Table 3.1 (Meinzer, 1927).

Table 3.1: Historic record of combined spring discharge at FRS.

Source	Date	Cumulative spring discharge (m ³ /s)
Davisson and Rose, 2014	Not given	34
Meinzer, 1927	Average over 19 months from 1912 and 1913	39
Meinzer, 1927	Lowest over 19 months from 1912 and 1913	35
Meinzer, 1927	Highest over 19 months from 1912 and 1913	45
Meinzer, 1927	9/9/1901	41
Meinzer, 1927	9/16/1902	44
Meinzer, 1927	9/11/1903	43
Meinzer, 1927	9/23/1910	42

Subsurface investigation has primarily focused on geothermal exploration and is localized to within the MLV Highlands area (Cumming & Mackie, 2007; Iovenitti & Hill, 1997). The shallow geothermal reservoir is present at elevations of 1500 – 1100m below the surface (Cumming & Mackie, 2007). The reservoir appears to be tightly sealed from the surface due to the lack of surface expression and the presence of a low permeability layer. This low permeability is likely the result of hydrothermal alteration and is evident in geophysical surveys performed for geothermal exploration (Burns et al., 2017). Additionally, a significant increase in geothermal gradient beneath the MLV Highlands area indicates the presence of this impermeable cap (*Information Sheet Order No. R5-2006*, 2006; Woodward, 2006). This cap formation could provide a localized bottom boundary for groundwater flow near MLV.

Additionally, the geology of MLV has been the subject of geologic investigation (Donnelly-Nolan, 2010; Donnelly-Nolan et al., 1991). MLV is a broad shield volcano that produced lava flows that ranged from basaltic to rhyolitic. One particular lava flow of hydrologic significance is the Giant Crater lava field, which occurred along the southwest flank of MLV and stretches 45 km to the

south, where the FRS emerge at the toe of the lava flow (Davisson & Rose, 2014; Donnelly-Nolan et al., 1991).

While past work provides valuable framework for the conceptual model, groundwater modeling and calibration further aids in the hydrogeological understanding of the MLVHA-FRS system. Additionally, calibrated hydraulic conductivity and aquifer thickness can be used to calculate the hydraulic response time, which is defined as the time it takes to observe a change in output following a change in input. In a diffusive system, this response time can be defined in terms of some characteristic length and diffusivity (Turcotte & Schubert, 1982; p. 157). Manga provides the following hydrologic analog where Kb/ϕ is the diffusivity term:

$$T_h = \frac{\phi}{2Kb} L^2 \quad \text{eq. 3-1}$$

where T_h is the hydraulic timescale, ϕ is the porosity, K is the hydraulic conductivity, b is the average thickness, and L is the characteristic length equal to the length of the aquifer (Manga, 1999). Other relationships exist for calculating the hydraulic timescale that use specific yield instead of porosity or differ from equation 3-1 by a factor of 3/2 (Gelhar, 1993). However, the equation above was used by Manga for fractured volcanic systems similar to the one under study in this project. For this application, the hydraulic timescale specifically refers to the length of time it takes to observe a change in spring discharge after a change in recharge occurs. Freeman noted a 1-2 year lag between changes in precipitation and changes in Fall River flow (Freeman, 2001). Knowing the timescale over which changes should be expected to propagate through the system is important for future work in understanding and protecting this valuable freshwater resource.

Methods

MODFLOW in GMS 10.3.4 was used to create the groundwater model. The conceptual model is shown in Figure 3.1. The model domain was based on work by Burns et al. (2017). The northern most boundary was modified to reflect an apparent groundwater divide as inferred from measured groundwater elevations (Iovenitti & Hill, 1997). A cell size of 300m x 300m was used

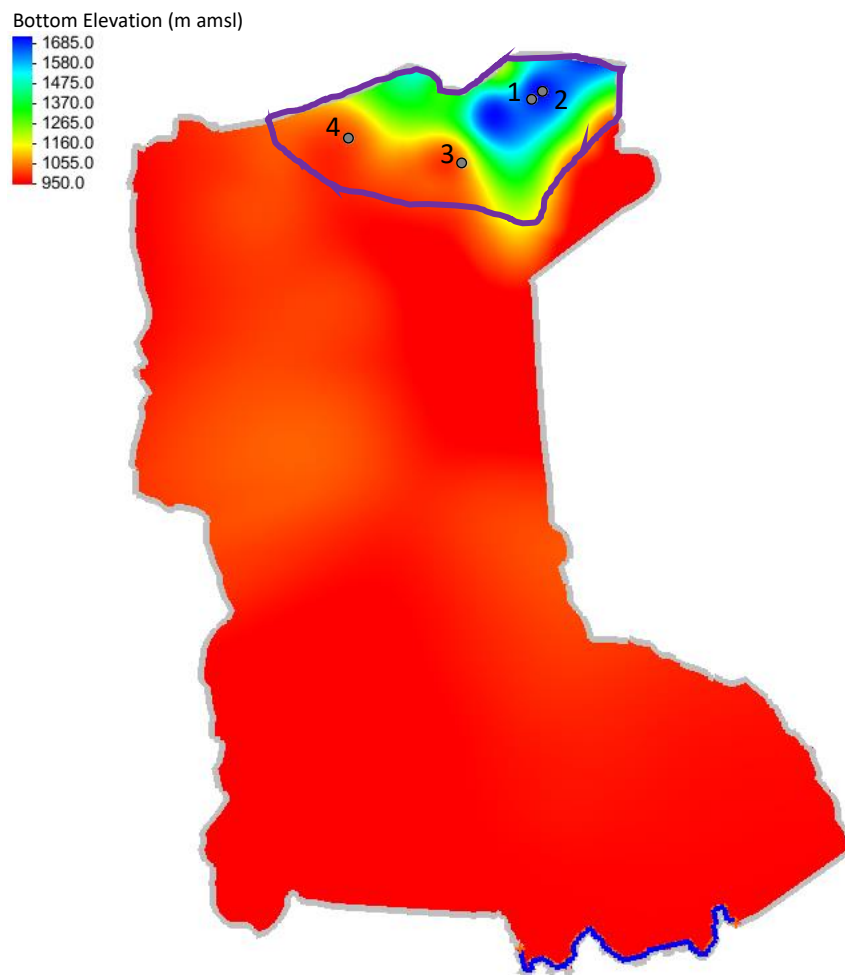


Figure 3.1: Conceptual model overview. Bottom elevation for an aquifer thickness of 50m is shown for the model domain. Specified head boundary for the springs are in blue. Outlined in purple is the upper zone of hydraulic conductivity. Observation points are shown in gray.

and the grid was rotated ~13% to better align with the direction of groundwater flow. The aquifer is assumed to be unconfined and the upper bound is assumed to be land surface as measured in a DEM. The bottom elevation in the Highlands area was assumed to be constant between model runs and based on the elevation of the top of the clay cap. This clay cap exists locally in the Highlands area due to the presence of the geothermal reservoir. Point values for elevation of the clay cap were estimated from magnetotellurics (MT) survey maps completed for geothermal exploration (Cumming & Mackie, 2007). Since little is definitively known about the thickness of the aquifer, lower elevation pseudo points were added assuming a linear decrease in bottom elevation between the Highlands area and FRS. The points from the MT surveys and the pseudo points were interpolated using the inverse distance method to approximate the bottom elevation. This interpolation was done for varying assumed aquifer thicknesses of 25m, 50m, 100m, 200m, 300m, and 400m, based on initial estimates discussed below.

The 20-year average of groundwater recharge from 1900 – 1920 simulated from the Basin Characterization Model (BCM) was calculated in ArcMap 10.3. The BCM is a water balance model that uses landscape, climate, and hydrologic variables and is discussed in detail in Chapter 4 (Flint & Flint, 2007). These years correspond with records of unimpaired flow for the FRS shown in Table 3.1 (Meinzer, 1927). The total recharge simulated by the BCM was 21 m³/s which represents ~60% of the historic cumulative spring discharge. In order to rectify this discrepancy, the BCM groundwater recharge was scaled so that the BCM output was equal to the historic discharge of 35 m³/s, while maintaining the distribution of groundwater recharge. This simplified approach will be improved upon in later work. The BCM raster was converted to points and interpolated in GMS. The interpolation process resulted in a discrepancy between

the total recharge from the BCM raster and the total interpolated recharge in GMS. A correction factor of 0.5 was applied to the interpolated values so that the total interpolated recharge was equal to the groundwater recharge from the BCM output.

The springs were modeled with a specified head boundary, where the head was set equal to the surface elevation. While some of the springs emerge from the toe of the lava field at a specific point, other areas of discharge are somewhat more diffuse. Therefore, the location of the springs was simplified by using an arc along the discharge area at the southern end of the site.

The groundwater model was calibrated to determine a range of hydraulic conductivity. It should again be emphasized that the purpose of this calibration is to use the model as a tool to explore the plausible range of bulk hydraulic conductivity values, rather than to definitively estimate the hydraulic conductivity at any point location. Observation data for groundwater head within the model domain was limited to four wells in the Highlands area. The model was manually calibrated to minimize both the mean absolute residual error and flooding within cells by keeping the groundwater levels below the land surface.

Initial estimates of hydraulic conductivity, using Darcy's Law, were used as a starting point in model calibration according to the following calculations:

$$K = \frac{Q}{bwi} \quad \text{eq. 3-2}$$

where K is the hydraulic conductivity, Q is the discharge, b is the average aquifer thickness, w is the aquifer width, and i is the hydraulic gradient (Fetter, 2001). The following equation is used to estimate the aquifer thickness:

$$b = \frac{T_{age}Q}{A\phi} \quad \text{eq. 3-3}$$

where b is the average thickness, T_{age} is the mean groundwater age, Q is the average discharge, A is the aquifer area, ϕ is porosity. The parameters in Table 3.2 and equation above were used to calculate an estimated mean aquifer thickness of 105 - 315m. Initial estimates of hydraulic conductivity from Darcy's law using the above calculated thickness range is 17 – 51 m/d. These initial values for hydraulic conductivity are consistent with literature values for lava flows (Heath, 1983). Model calibration of hydraulic conductivity to improve these estimates was performed manually. Because the aquifer dimensions are largely unknown, calibration was repeated for varying values of aquifer thickness. Aquifer thickness of 25m, 50m, 100m, 200m, 300m, and 400m were evaluated based off of the initial estimates of aquifer thickness from above. The hydraulic conductivity from the calibrated model was then used to estimate the

Table 3.2: Values for parameters used to calculate the initial estimates for hydraulic conductivity and aquifer thickness. Initial estimates were used to as a starting point for model calibration.

<i>Parameter</i>	<i>Value</i>	<i>Unit</i>	<i>Sources</i>
Porosity	10 - 30	%	(Ingebritsen et al., 2016; Navarre-Sitchler et al., 2009; Saar & Manga, 1999)
Area	1400	km ²	Model domain
Discharge	35	m ³ /s	(Meinzer, 1927)
Age	40	years	CFC apparent age
Average Thickness	105 - 315	m	Calculated
Width	28000	m	Approximated from model domain
Change in Head	1000	m	Estimated (Iovenitti and Hill, 1997)
Hydraulic Gradient	0.02	m/m	Estimated
Hydraulic Conductivity	17 - 51	m/d	Calculated

hydraulic response time. The calculated hydraulic response time was compared to that noted by Freeman from observed cumulative spring discharge and precipitation in order to calibrate the effective porosity (Freeman, 2001).

Results and Discussion

During calibration, use of a single bulk hydraulic conductivity turned out to be too simple of an approach for this aquifer system. Doing so does not reproduce the steep hydraulic gradient in the Highlands area, shown in Figure 3.2. For this reason, the model domain was further split into two zones of hydraulic conductivity; an upper zone in the Highlands area with a lower hydraulic

conductivity, and a lower zone throughout the rest of the domain shown in Figure 3.1. This representation is plausible as the Highlands area has more developed soils, as well as more alteration of rock from the geothermal reservoir, resulting in a lower hydraulic conductivity, compared to the highly fractured exposed lava fields along the remaining portion of the site from the Highlands area down to FRS. Again, this was done to accommodate the steep hydraulic gradient.

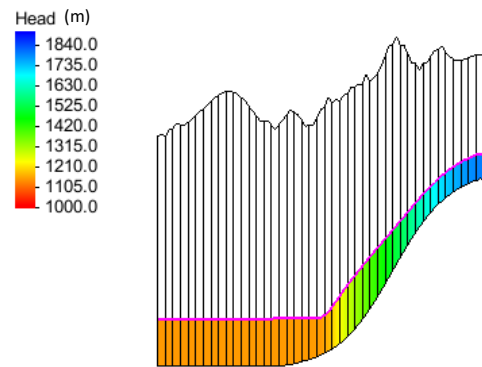


Figure 3.2: Selected cross section showing the groundwater head along the steep gradient in the Highlands.

It is likely, however, that some sort of structural controls are causing the steep gradient. When examining the elevation and the modeled groundwater head at the Paynes Springs, the groundwater table is 160 – 260m below the elevation of Paynes Springs. Thus, it is probable that Paynes Springs are perched due to geologic constraints to flow. Of interest to this project, however, are the bulk parameters of the aquifer. Therefore, the steep gradient was accommodated by using a lower hydraulic conductivity in the upper zone rather than including uncertain and complicated structural controls to flow, such as those that might be hydrologically relevant to Paynes Springs.

Table 3.3: Calibrated hydraulic conductivity and calculated hydraulic timescale.

Thickness (m)	Hydraulic Conductivity (m/d)		Porosity	Hydraulic Timescale (yr)
	Upper Zone	Lower Zone		
25	0.7	500	0.1	22
			0.3	65
50	0.6	400	0.1	24
			0.3	73
100	0.7	300	0.1	9
			0.3	28
200	0.5	300	0.1	8
			0.3	25
300	0.7	100	0.1	16
			0.3	49
400	0.7	100	0.1	7
			0.3	21

The calibrated hydraulic conductivities for both the upper and lower zones are shown in Table 3.3. The mean error (Tables 3.4 – 3.9) is rather large for all thicknesses. However, with little additional observation data for hydraulic head and the bottom boundary of the system, these values still represent a suitable estimate of bulk hydraulic conductivity in the two zones. It should be noted again that for the varying thicknesses, only the thickness of the southern portion of the aquifer was manipulated by lowering the aquifer bottom. The bottom of the

Table 3.4: Error summary for aquifer thickness = 25m, upper zone hydraulic conductivity = 0.7 m/d and lower zone hydraulic conductivity = 500 m/d.

Observation Point	Observed Head (m amsl)	Calculated Head (m amsl)	Percent Difference (%)	Mean Absolute Residual Error	Mean Residual Error
1	1760	1809	-2.77	55.31	30.94
2	1826	1809	0.91		
3	1450	1449	0.05		
4	1543	1388	10.06		

Table 3.5: Error summary for aquifer thickness = 50m, upper zone hydraulic conductivity = 0.6 m/d and lower zone hydraulic conductivity = 400 m/d.

Observation Point	Observed Head (m amsl)	Calculated Head (m amsl)	Percent Difference (%)	Mean Absolute Residual Error	Mean Residual Error
1	1760	1828	-3.86	56.97	7.33
2	1826	1828	-0.11		
3	1450	1478	-1.93		
4	1543	1414	8.36		

Table 3.6: Error summary for aquifer thickness = 100m, upper zone hydraulic conductivity = 0.7 m/d and lower zone hydraulic conductivity = 300 m/d.

Observation Point	Observed Head (m amsl)	Calculated Head (m amsl)	Percent Difference (%)	Mean Absolute Residual Error	Mean Residual Error
1	1760	1809	-2.77	55.35	30.96
2	1826	1809	0.90		
3	1450	1449	0.06		
4	1543	1388	10.06		

Table 3.7: Error summary for aquifer thickness = 200m, upper zone hydraulic conductivity = 0.5 m/d and lower zone hydraulic conductivity = 300 m/d.

Observation Point	Observed Head (m amsl)	Calculated Head (m amsl)	Percent Difference (%)	Mean Absolute Residual Error	Mean Residual Error
1	1760	1855	-5.40	71.45	-20.00
2	1826	1855	-1.59		
3	1450	1509	-4.07		
4	1543	1441	6.61		

Table 3.8: Error summary for aquifer thickness = 300m, upper zone hydraulic conductivity = 0.7 m/d and lower zone hydraulic conductivity = 100 m/d.

Observation Point	Observed Head (m amsl)	Calculated Head (m amsl)	Percent Difference (%)	Mean Absolute Residual Error	Mean Residual Error
1	1760	1810	-2.84	53.49	20.94
2	1826	1811	0.82		
3	1450	1465	-1.03		
4	1543	1409	8.68		

Table 3.9: Error summary for aquifer thickness = 400m, upper zone hydraulic conductivity = 0.7 m/d and lower zone hydraulic conductivity = 100 m/d.

Observation Point	Observed Head (m amsl)	Calculated Head (m amsl)	Percent Difference (%)	Mean Absolute Residual Error	Mean Residual Error
1	1760	1810	-2.81	54.09	25.21
2	1826	1810	0.86		
3	1450	1458	-0.57		
4	1543	1400	9.26		

aquifer in the Highlands area is geologically constrained by the clay cap overlaying the geothermal system and was held constant during the calibration and sensitivity analysis.

In general, the range for hydraulic conductivity for each thickness was bounded by accommodating the steep gradient, reducing the number of flooded cells, and minimizing error between observed and modeled points. A hydraulic conductivity value that was too high would result in excessive flooding of cells in the model domain. Values that were too low would interfere with the model's ability to maintain the steep water-level gradient in the Highlands area. The upper zone was extremely sensitive to changes in hydraulic conductivity due to the steep gradient, thus small changes to either the upper or lower zone hydraulic conductivity would affect the error observed between the model and observation points. This additionally aided in providing an upper and lower bound for the range of possible values.

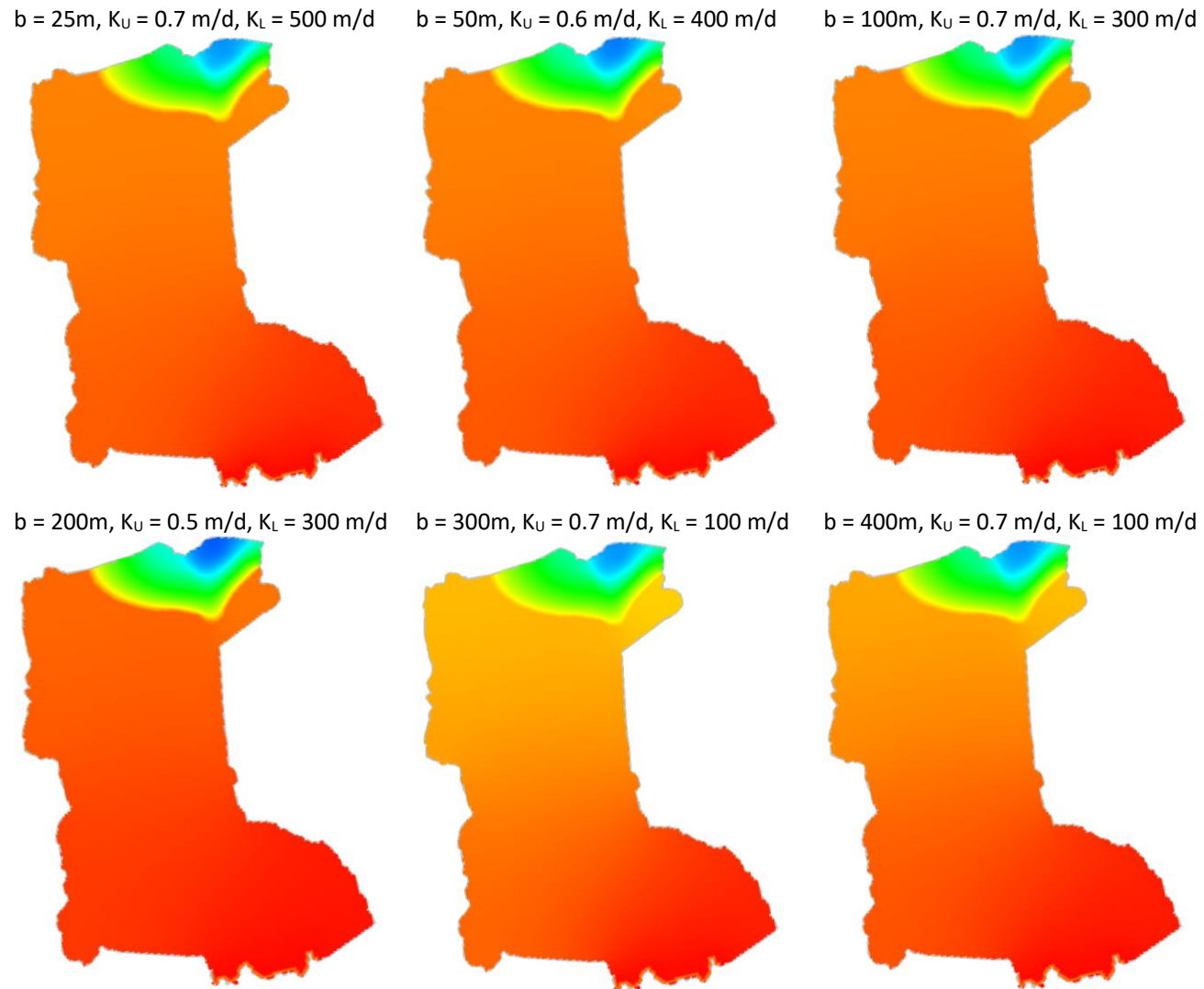


Figure 3.3: Groundwater head for the optimal calibrated solution of upper zone (K_U) and lower zone (K_L) hydraulic conductivity for each aquifer thickness (b).

The optimal solution for each of the thicknesses evaluated is shown in Figure 3.3. Overall, regardless of the aquifer thickness, the upper zone hydraulic conductivity is on the order of 10^{-1} m/d and the lower zone hydraulic conductivity is 10^2 m/d. These values within the range of literature values for volcanic systems of $10^{-2} - 10^4$ m/d (Heath, 1983).

Of the various combinations of aquifer thickness and hydraulic conductivity evaluated, the mean absolute residual error was similar for an aquifer thickness of 25m, 50m, 100m, 300m and 400m with the lowest error for a thickness of 300m with a corresponding hydraulic conductivity in the upper and lower zones of 0.7 m/d and 100 m/d respectively. Older volcanic rocks underlie the Giant Crater lava flows. Those rocks are may have undergone significant weathering, reducing their conductivities and potentially limiting flow. Thus, it may be more appropriate to assume a thickness less than 300 m. Based on this geologic interpretation and the error from the calibrations, the thickness is likely closer to 25 – 100m, with an upper zone hydraulic conductivity from 0.6 – 0.7 m/d and a lower zone hydraulic conductivity between 300 – 500 m/d.

The hydraulic timescale from the Highlands area, specifically the edge of the upper hydraulic conductivity zone, to FRS was calculated in Table 3.3 for different porosity values for volcanic materials based on literature (Ingebritsen et al., 2016; Navarre-Sitchler et al., 2009; Saar & Manga, 1999). Differences in porosity has a noticeable impact on the calculated hydraulic timescale. Using the initial porosity values of 0.1 and 0.3, the hydraulic timescale was <25 years and <80 years respectively. These values are much greater than the 1-2 year lag time in the

observation data from Freeman (2001). Using the observed hydraulic timescale of 1-2 years and the calibrated hydraulic conductivities for each aquifer thickness, the porosity was then calculated (Table 3.10). Thus, it is more likely that the effective porosity is on the order of 0.01 rather than 0.1. Additionally, while Freeman (2001) notes a lag time of 1-2 years between precipitation and discharge which showed a 15-year periodicity, while unlikely, this interpretation could potentially be a cycle off. Consequently, the lag time could alternatively be 15 years (Table 3.10).

Table 3.10: Estimated porosity using calibrated hydraulic conductivity and aquifer thickness considering either a 1-2 versus a 15-year hydraulic timescale.

Lower Zone K (m/d)	Aquifer Thickness (m)	Hydraulic Timescale (yr)	Porosity
500	25	1	0.005
400	50	1	0.007
300	100	1	0.011
500	25	2	0.009
400	50	2	0.014
300	100	2	0.022
500	25	15	0.068
400	50	15	0.108
300	100	15	0.162

The calibrated range of aquifer thickness and porosity were used to estimate the travel time from Paynes Springs to FRS (Table 3.11) and were compared to the CFC ages from Ch 2. Travel times are on the order of 1 – 10 years. It should be noted that the total recharge was used in the calculations, thus this range may be an underestimation of travel time. From Ch 2, the CFC groundwater age at Paynes Springs is ~30 years and ~40 years at FRS. Overall, this indicates slow transport in the Highlands area (~30 years) and swift travel times (~10 years) in the high permeability material from Paynes Springs down to FRS, where the groundwater age is ~40 years.

Table 3.11: Travel time from Paynes Springs to FRS for calibrated aquifer thickness and porosity.

Thickness (m)	Porosity	Travel Time (yr)
25	0.01	0.29
50	0.01	0.57
100	0.01	1.14
25	0.05	1.43
50	0.05	2.85
100	0.05	5.71
25	0.1	2.85
50	0.1	5.71
100	0.1	11.42

Conclusions and Future Work

Due to the steep hydraulic gradient in the Highlands area, two zones of hydraulic conductivity were simulated with an upper zone having a hydraulic conductivity on the order of 10^{-1} m/d and the lower zone equal to 10^2 m/d. Based on the mean residual error for the configurations examined and site geology, the combination of an aquifer thickness between 25 – 100m and an upper and lower zone hydraulic conductivity of 0.6-0.7 m/d and 300 – 500 m/d, respectively, appear to account for observed hydrogeologic conditions. While defining an appropriate aquifer thickness resulted in a somewhat broad range from 25m – 100m, the corresponding calibrated hydraulic conductivities are within the same order of magnitude. Using the hydraulic timescale of 1-2 years, the bulk effective porosity is likely on the order of 0.01 rather than initial estimates of 0.1. Estimates of travel time from Paynes Springs to FRS using calibrated porosity and aquifer thickness are on the order of 1-10 years, indicating rapid transport through the permeable material from the Highlands area down to FRS.

Additional understating of groundwater recharge is necessary for further modeling efforts, as groundwater recharge from the BCM accounted for only ~60% of the total historic spring discharge. Further observation data (measured groundwater head) would be beneficial to improve the calibration. This would especially be useful along the slope of the Highlands area with the steep hydraulic gradient, as well as in within the lava field itself within the lower zone of hydraulic conductivity. Aquifer testing for K at multiple locations would additionally aid in the calibration process. Finally, a geologic investigation of the porosity of this particular volcanic system would greatly improve estimates of the hydraulic timescale. This additional work would further elucidate the hydrogeologic properties and understanding of the system.

References

- Burns, E. R., Zhu, Y., Zhan, H., Manga, M., Williams, C. F., Ingebritsen, S. E., & Bunham, J. B. (2017). Thermal effect of climate change on groundwater-fed ecosystems. *Water Resources Research*, 3341–3351. <https://doi.org/10.1002/2016WR020007>. Received
- Cumming, W., & Mackie, R. (2007). MT Survey for Resource Assessment and Environmental Mitigation at the Glass Mountain KGRA. Energy Research and Development Division Final Project Report.
- Davisson, M. L., & Rose, T. P. (2014). Recharge and Flow in the Medicine Lake Volcano – Fall River Springs Groundwater Basin, California. *Environmental Forensics*, 66–77. <https://doi.org/10.1080/15275922.2013.873097>
- Donnelly-Nolan, J. M. (2010). Geologic Map of Medicine Lake Volcano, Northern California. USGS.
- Donnelly-Nolan, J. M., Champion, D. E., Grove, T. L., Baker, M. B., Taggart, J. E., & Bruggman, P. E. (1991). The Giant Crater Lava Field: Geology and geochemistry of a compositionally zoned, high-alumina basalt to basaltic andesite eruption at Medicine Lake Volcano, California. *Journal of Geophysical Research: Solid Earth*, 96(B13), 21843–21863. <https://doi.org/10.1029/91JB01901>
- Fetter, C. W. (2001). *Applied Hydrology* (4th ed.). Upper Saddle River: Prentice Hall.
- Flint, A., & Flint, L. (2007). Application of the basin characterization model to estimate in-place recharge and runoff potential in the Basin and Range carbonate-rock aquifer system, White Pine

- County, Nevada, and adjacent areas in Nevada and Utah. US Geological Survey Scientific Investigations Report 2007-5099.
- Freeman, G. J. (2001). The Impacts of Current and Past Climate on Pacific Gas & Electric 's 2001 Hydroelectric Outlook (pp. 21–38).
- Gelhar, L. W. (1993). Stochastic subsurface hydrology. Prentice-Hall, Englewood Cliffs, N.J.
- Heath, R. C. (1983). Basic Ground-Water Hydrology. Basic Ground-Water Hydrology. Resont, VA. Information Sheet Order No. R5-2006. (2006). Retrieved from https://www.waterboards.ca.gov/rwqcb5//board_decisions/tentative_orders/0605/calpine/calpine-info.pdf
- Ingebritsen, S. E., Bergfeld, D., Clor, L. E., & Evans, W. C. (2016). The Lassen hydrothermal system. *American Mineralogist*, 101(2), 343–354. <https://doi.org/10.2138/am-2016-5456>
- Iovenitti, J. L., & Hill, D. G. (1997). Baseline hydrogeology evaluation report for Telephone Flat geothermal project Medicine Lake, California. Emeryville, CA. Retrieved from https://books.googleusercontent.com/books/content?req=AKW5Qad9SySHToSdN_BO07WJvgDJj7yUtasyPszA8B2oZdFhiY_PQ4q33I6DPvtVQrdLgv5CvzgDE9SsvpgKjWeM9Zxwlfmqb-xFYp8ANPDZE248QQ70u8Bltb63Bi6nbCiaVGRo2UzHVC8zu1AHwOdCeU4I9qXfjAM-3QSAH1_a5-NexKaYuFRF9L1_JDZx0dxW-zQ-d
- Manga, M. (1999). On the timescales characterizing groundwater discharge at springs. *Journal of Hydrology*, 219(1–2), 56–69. [https://doi.org/10.1016/S0022-1694\(99\)00044-X](https://doi.org/10.1016/S0022-1694(99)00044-X)
- Meinzer, O. E. (1927). Large springs in the United States. Geological Survey Water-Supply Paper 557. Washington, D. C.
- Navarre-Sitchler, A., Steefel, C. I., Yang, L., Tomutsa, L., & Brantley, S. L. (2009). Evolution of porosity and diffusivity associated with chemical weathering of a basalt clast. *Journal of Geophysical Research*, 114(F2), F02016. <https://doi.org/10.1029/2008JF001060>
- Palmer, P. C., Gannett, M. W., & Hinkle, S. R. (2007). Isotopic characterization of three groundwater recharge sources and inferences for selected aquifers in the upper Klamath Basin of Oregon and California, USA. *Journal of Hydrology*, 336(1–2), 17–29. <https://doi.org/10.1016/j.jhydrol.2006.12.008>
- Saar, M. O., & Manga, M. (1999). Permeability-porosity relationships in vesicular basalts. *Geophysical Research Letters*, 26(1), 111–114.
- Turcotte, D. L., & Schubert, G. (1982). *Geodynamics: Applications of Continuum Physics to Geological Problems*. New York: John Wiley & Sons, Inc.
- Woodward, P. (2006). Comments on placement of monitoring wells near geothermal production well No. 31-17, Telephone Flat geothermal exploration and development project, Siskiyou County, California. Redding, CA.

Ch 4 – Basin Characterization Model Analysis

Introduction

The Basin Characterization Model (BCM) is a water balance model that uses climate and landscape information to simulate a variety of climate and hydrologic variables (Figure 4.1). The model output has been widely used in California and the Great Basin at both regional and watershed scales to evaluate possible impacts of climate change (Flint and Flint, 2007; Flint and Flint, 2012; Flint and Flint, 2007; Heller et al., 2015; Micheli et al., 2012; Thorne et al., 2015). The BCM uses monthly air temperatures and precipitation from PRISM as inputs. PET is calculated using the Priestley-Taylor equation (Priestley & Taylor, 1972) with hourly solar radiation, topographic shading, and PRISM air temperature as inputs. The PET is also adjusted for cloudiness and aggregated to a monthly timescale. Snowfall and snowpack is modeled within the BCM using the National Weather Service Snow-17 model (Anderson, 1976). Basin outflow in the BCM refers to the sum of recharge and runoff where recharge in the BCM is the amount of water that percolates below the root zone and runoff is the amount of water that exceeds the total storage as well as any rejected recharge. In regard to further discussion below, the terms basin outflow and recharge are used interchangeably to mean the total amount of water that reaches the groundwater table defined as the sum of runoff and recharge within the BCM (J. Thorne et al., 2012). The BCM was calibrated using stream gage data from 138 unimpaired watersheds throughout California (L. E. Flint et al., 2013). The BCM does not route streamflow, but due to the lack of surface runoff, as well as the unimpaired nature of the site, the MLVHA-FRS system is a suitable locale for using the BCM output.

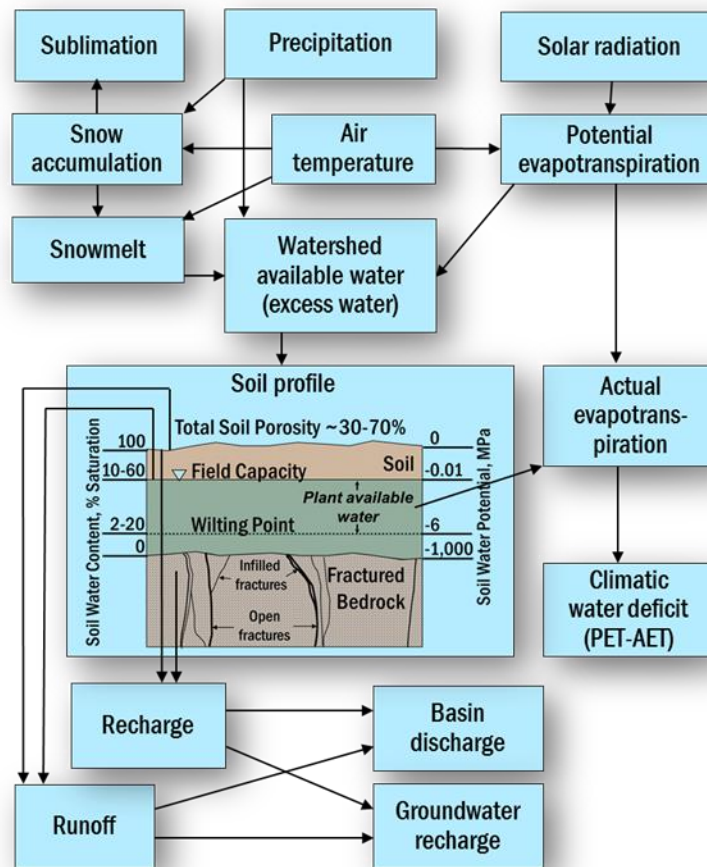


Figure 4.1: Schematic of processes modeled by the BCM (Thorne et al., 2012).

Currently the primary source of recharge for MLVHA is snowmelt (Davisson and Rose, 2014).

With increasing temperatures, multiple studies indicate a decline in snow dominated precipitation areas across the western US (Freeman, 2012; Lute, Abatzoglou, and Hegewisch, 2015; Lynn, 2015; Safeeq et al., 2016). In one study, an increase in temperature by 1 degree C resulted in decrease in snow to precipitation proportion by 10-15% in the Northern Sierra, Klamath Mountains and western Cascades (Safeeq et al., 2016). The MLVHA-FRS system has already been observed to respond to changes in precipitation amount. Discharge from the springs fluctuates on a 14 - 16 year cycle that appears to mirror long term precipitation

variations (Freeman, 2001). Thus, there is concern that changing precipitation type may influence the system hydrology and ultimately spring discharge.

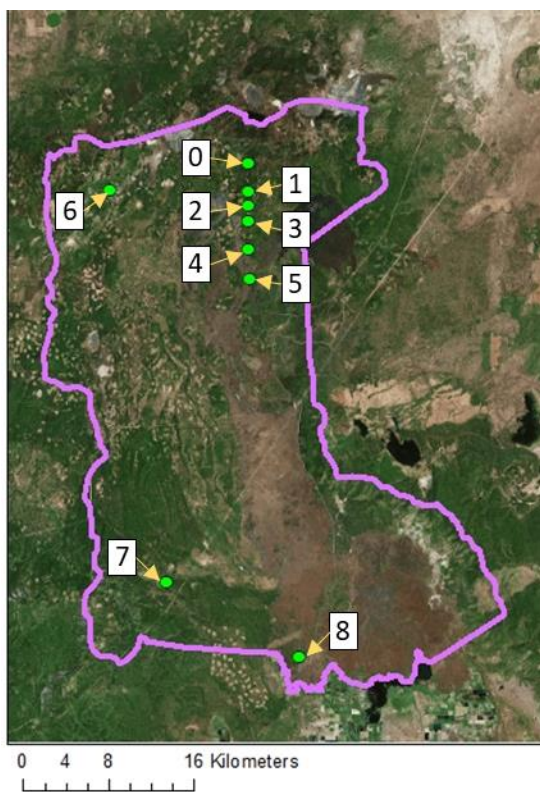
Methods

To evaluate the impact of climate change on the MLVHA-FRS system, monthly outputs at various point locations were examined from BCM simulation under historic conditions and GFDL A2, a warmer and drier projected future. The time period associated with the historic scenario is from 1900 – 2010. The inputs for this historical BCM simulation are based on downscaled PRISM data using the gradient-inverse distance squared (GIDS) method. It is best practice to evaluate more than just one GCM in order to evaluate a range of possible outcomes (Lynn et al., 2015), and so simulations of responses to climate changes from additional GCMs will be analyzed at a later time. The selected projected scenario is in keeping with recommendations from Lynn (2015), who evaluated historic output for several GCMs on a set of metrics specifically relating to California's climatic and hydrologic variability. The projected scenario spans from 2011 – 2099.

The output variables from the BCM output used here are precipitation, snowfall (as snow water equivalent or SWE), actual evapotranspiration (AET) and groundwater recharge. An important distinction should be noted regarding this latter term. BCM defines groundwater recharge as the combination of water that has infiltrated below the root zone, referred to as recharge, as well as a portion of runoff that is controlled by the bedrock permeability. The BCM doesn't appear to accommodate the high permeability of the rock and soil at this site, as the recharge values are smaller than expected, and runoff much greater. Field observations indicate that there is virtually no surface water flow and it is assumed that any runoff quickly infiltrates into the permeable exposed bedrock. Thus, for the purposes of this study, the total runoff was

combined with the recharge term. The sum of runoff and recharge is what is meant by “groundwater recharge” for the purposes of this work, per Flint and Flint’s definition (L. Flint & Flint, 2007).

Points 0 – 5 were selected along a transect that spans the area of transition from snow to rain from the historic to projected scenarios in the Highlands area (Figure 4.2, Table 4.1). This transition area was defined by examining 30-year average historic April 1st snowpack for 1951 – 1980, and 1981 – 2010. The snowpack output was normalized by the total precipitation for that time period. The difference between historic and projected normalized April 1st snowpack was compared for the projected scenario. The location chosen for the transect was selected to capture the greatest difference between historic and projected normalized April 1st snowpack



for the projected scenario. The remaining points were selected to capture variation across the study area at different elevations. Point 6 is located in the upper elevation area to the west of MLV Highlands area. Point 7 is at a lower elevation area with relatively high average precipitation and is located west of FRS. Point 8 is the lowest in elevation with the lower amounts of precipitation and near FRS (Figure 4.2, Table 4.1).

Figure 4.2: BCM analysis point locations.

Prior to additional analysis, the BCM output was evaluated against limited observation data to assess the appropriateness of using its outputs to evaluate changes to the system. Two stations were identified at the site; one near Medicine Lake (SnowLite station ID MED) and one in Fall River Mills, CA near FRS (NWS Cooperative Network station number 042964-2). Temperature, snow water equivalent (SWE) and precipitation records were available at the two stations. The BCM output was examined for changes over time and for correlation to assess possible shifts in relative amounts of recharge and associated climate variables. Additionally, cumulative output was analyzed to elucidate the timing of recharge and related climate variables throughout the year.

Table 4.1: Location and description of point locations for BCM output analysis.

Location Name	General Location	X (m)	Y (m)	Elevation (m)
Pt0	MLVH	-134095.823	392978.973	2013
Pt1	MLVH	-134015.893	390314.671	1800
Pt2	MLVH	-134149.109	388929.234	1710
Pt3	MLVH	-134042.536	387570.440	1665
Pt4	MLVH	-134095.823	384932.781	1547
Pt5	MLVH	-134015.893	382188.549	1468
Pt6	West of MLVH	-146991.046	390447.886	1732
Pt7	West of FRS	-140852.037	353696.992	1230
Pt8	Near FRS	-129393.008	346614.677	1026

LOWESS, or locally weighted scatterplot smoothing, was used as a middle smoothing method to evaluate changes in the output over time. LOWESS, is an iterative, robust, nonparametric smoothing technique (Helsel & Hirsch, 2002). This method involves computing a new y-value using a weighted least squares (WLS) regression at each x-value. First, the data is split up into “windows,” the size of which is controlled by a smoothing factor, f , which ranges from 0 to 1 and describes the fraction of the data to be used as the smoothing window. A value of $f = 0.21$ was chosen to correspond with periodicity observed in discharge and precipitation data, discussed in

detail later (Freeman, 2001). The WLS regression is then performed within each of these windows. There are two different weighing factors that are used in the calculations. The first is the distance from the x-values within the window to the x-value for which the new y-value is being calculated. After the first iteration, a second weight is incorporated in determining the WLS regression. This weight is relative to the difference in the magnitude of the residuals from the previous iteration (Cleveland, 1979). The curve produced represents the middle of the data or a weighted average of sorts. These methods were applied at each point for total yearly groundwater recharge, actual evapotranspiration (AET), yearly total precipitation and snowfall (SWE), as well as normalized total yearly recharge and normalized total yearly AET. Normalization refers to normalizing by the total yearly precipitation and the yearly timescale refers to calendar year, as opposed to water year.

The Theil-Sen, also known as the Kendall-Theil, line was also evaluated for each of the variables mentioned above to determine whether or not a statistically significant trend is present in the output. A positive slope indicates an increasing trend and a negative slope, a decreasing trend. The slope of the Theil-Sen line is the median of all possible slopes between all x,y points. The y-intercept is calculated from this slope, the median of the x-values and the median of the y-values (Helsel & Hirsch, 2002). A trend in the output was determined based on the whether the slope is statistical different from zero at the 95% confidence interval.

Also examined was data at the basin, or watershed, scale. The publicly available 30-year average BCM output was summed over the watershed area to determine cumulative volumes of water for precipitation, groundwater recharge, and AET. Output for April 1st snowpack was also

evaluated, as well as normalized AET and normalized groundwater recharge. Changes in these summary values were evaluated over time from the historic to projected time period.

Correlation analysis was performed on the following combination of variables: total yearly AET and total yearly groundwater recharge, total yearly precipitation and total yearly groundwater recharge, and snowfall (SWE) and total yearly groundwater recharge. The correlation coefficient was assessed from each relationship to provide a measure of the strength of association between the two variables. Pearson's r was used as the correlation coefficient which provides a measure of the linear relationship between two variables (Helsel & Hirsch, 2002).

Yearly cumulative plots were created for AET, groundwater recharge, snowfall and precipitation. Monthly output was averaged over 30-year periods for the both the historic and projected scenario. These plots were created to assess changes in the timing of climate variables throughout the year.

Results and Discussion

BCM Output and Observation Data

The comparison of temperature from the observation stations with the BCM output was difficult due to the lack of continuous and reliable temperature observations at Medicine Lake, however, total monthly precipitation are relatively highly correlated ($r = 0.81$). Additionally, daily minimum and maximum temperatures, and precipitation yielded high correlation at the Fall River Mills location as shown in Figure 4.3. The precipitation output was also analyzed for the 14-16 year periodicity in 5-year moving average mentioned by Freeman (2001). This periodicity

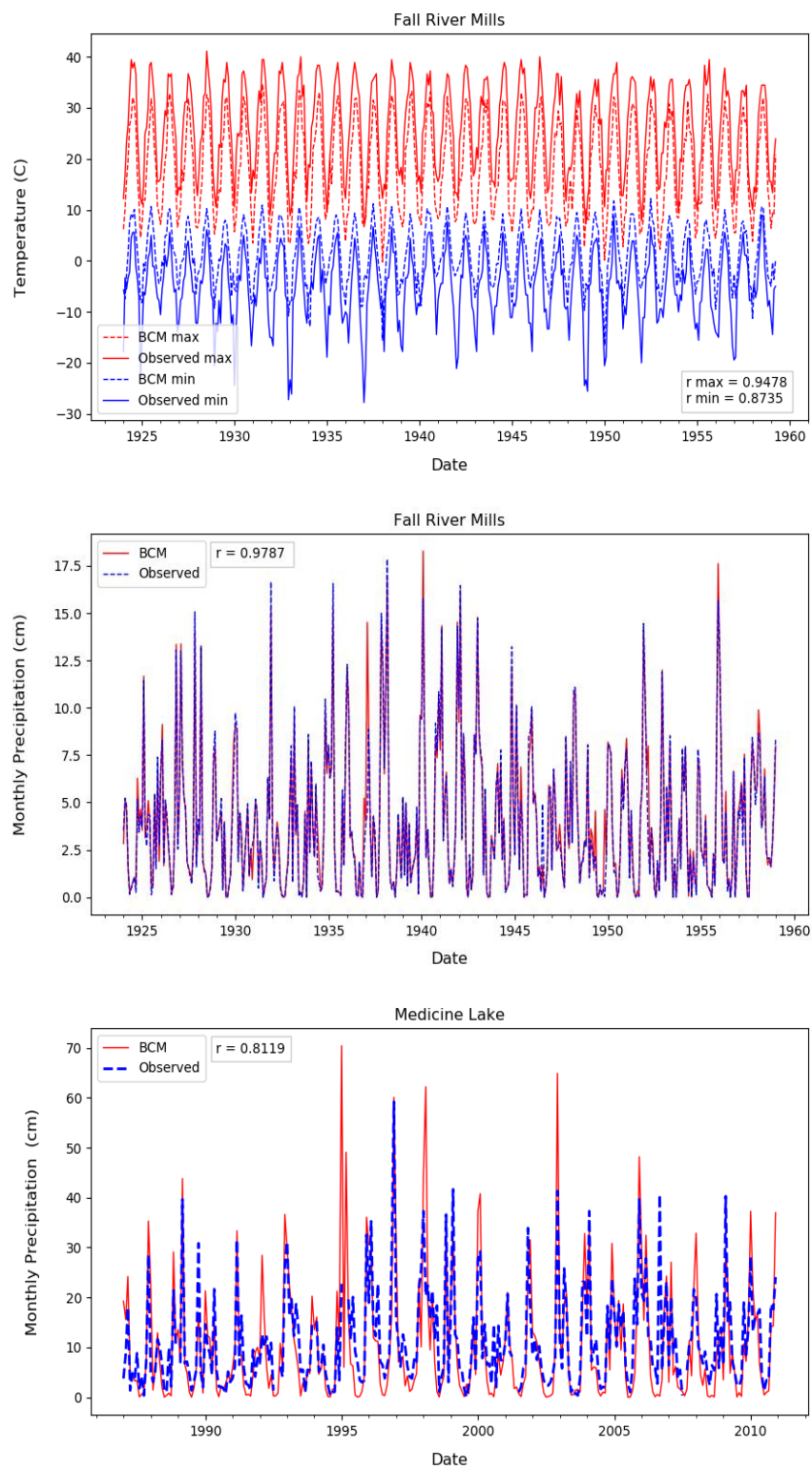


Figure 4.3: Comparison of BCM output and observation data from Medicine Lake and Fall River Mills.

was preserved in the historic BCM precipitation output (Figure 4.4). As previously mention, the smoothing factor, f , for LOWESS smoothing was based on this combined periodicity of the 5-year moving average and 16-year periodicity within that moving average. Furthermore, as discussed in Ch 3, the cumulative groundwater recharge, defined as the sum of recharge and runoff from the BCM, within the site boundary represents only ~60% of the historic range of spring discharge measurements. Thus, the following analysis applies only to this portion of the groundwater recharge, as 40% of the total groundwater recharge is not accounted for with the BCM.

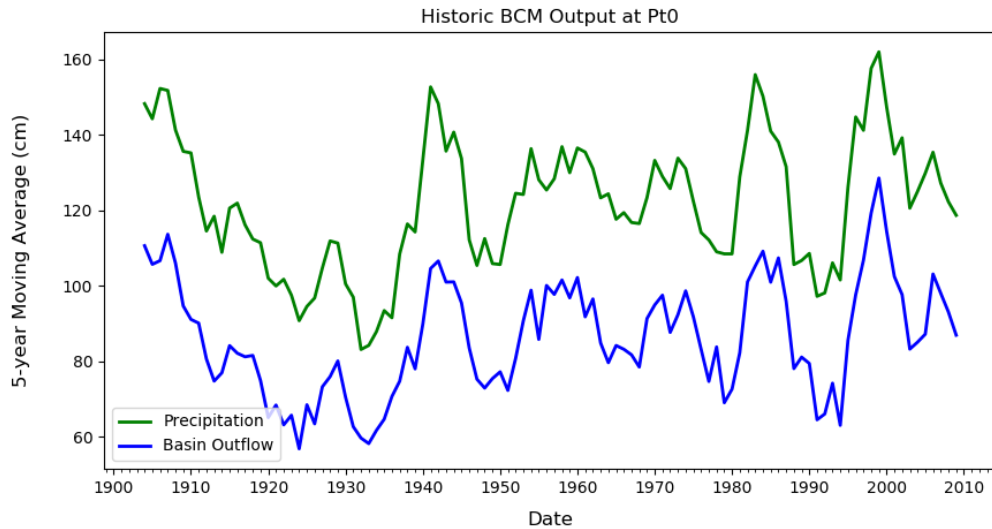


Figure 4.4: Historical BCM output at Pt0 for precipitation and basin outflow.

Historical Scenario

In examining the climate variables, changes to the water balance “input” (precipitation) were evaluated along with the remaining climate variables to assess changes in amount and contribution in balancing the overall water budget as follows:

$$\text{Precipitation} = \text{AET} + \text{Groundwater Recharge} + \text{Sublimation} \quad \text{eq.4-1}$$

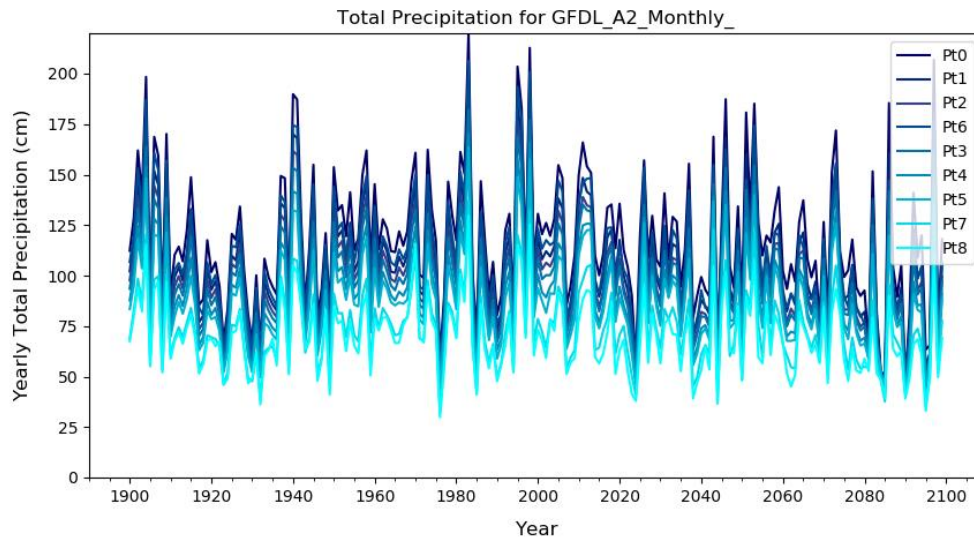


Figure 4.5: Total yearly precipitation during the historic and projected time periods at all point locations. Point locations in legend are displayed in order of decreasing elevation.

No statistically significant trend in yearly total precipitation was found at any point during the historic period. Thus, precipitation has remained relatively stable throughout the historic period amidst large multi-year fluctuations characterized by Freeman (2001) as following roughly a 14 – 16 year cycle (Figure 4.5). This is also shown in Figure 4.6 at the watershed scale. The average yearly total precipitation over the watershed is 85.3 cm/yr. Geographically, the total amount of precipitation decreases with decreasing elevation, as shown in Figure 4.5 so that more precipitation falls in the Highlands area than near FRS.

No trend was found for yearly total AET, snowfall and groundwater recharge at any points during the historical period. This indicates that each of these variables are relatively consistent throughout the historic time period. For the normalized yearly total AET a very slight, but statistically significant declining trend was found at all points except point 3, with magnitude of $1.0 - 4.0 \times 10^{-4} \text{ yr}^{-1}$. The normalized yearly total groundwater recharge increased slightly at all

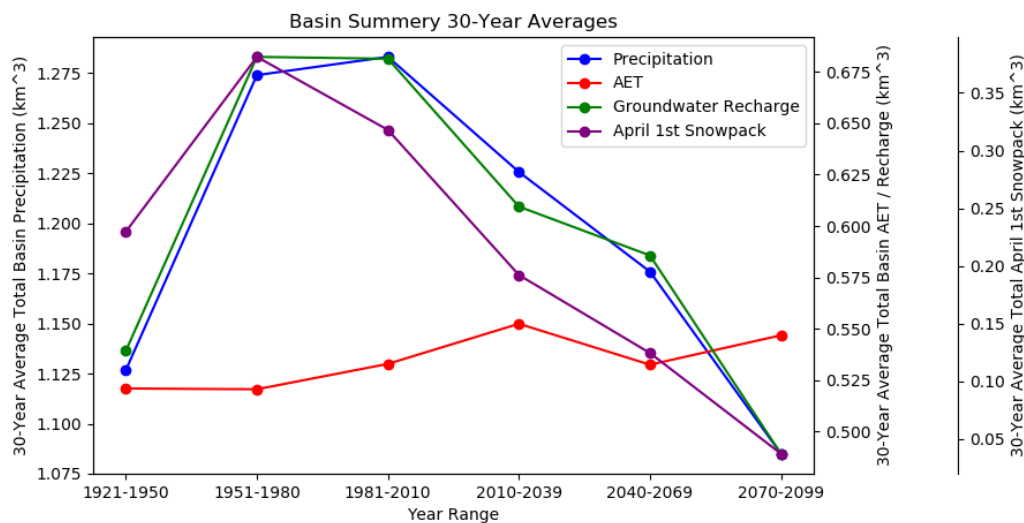


Figure 4.6: Total volume over the watershed for precipitation, AET, groundwater recharge and April 1st snowpack for 30-year averages for historic and projected scenarios.

points from $1.0 - 7.0 \times 10^{-4} \text{ yr}^{-1}$. The normalized output can be thought of as the efficiency of precipitation to result in the variable being normalized. For example, higher normalized output indicates that for years with a lot of precipitation, more precipitation is partitioned into the normalized variable. Therefore, the proportion of precipitation that is becoming AET decreases, while the amount that becomes recharge increases during the historic time period. However, the magnitudes of these trends are very small and indicates that there is relatively little change during the historic time period in the efficiency of precipitation to produce AET and recharge. Furthermore, this is observed through visual assessment of the LOWESS smoothed values, which are relatively consistent throughout time. For example, normalized AET is shown in Figure 4.7 for point 3. At the overall basin scale, the average for yearly total AET and groundwater recharge over the water year are respectively 36.5 cm/yr and 44.1 cm/yr and the average April 1st snowpack is 21.5 cm. The overall water budget, as presented in the equation above, balances with only a +/- 0.5% difference between the total “input” (precipitation) and “output” (AET, groundwater recharge and sublimation).

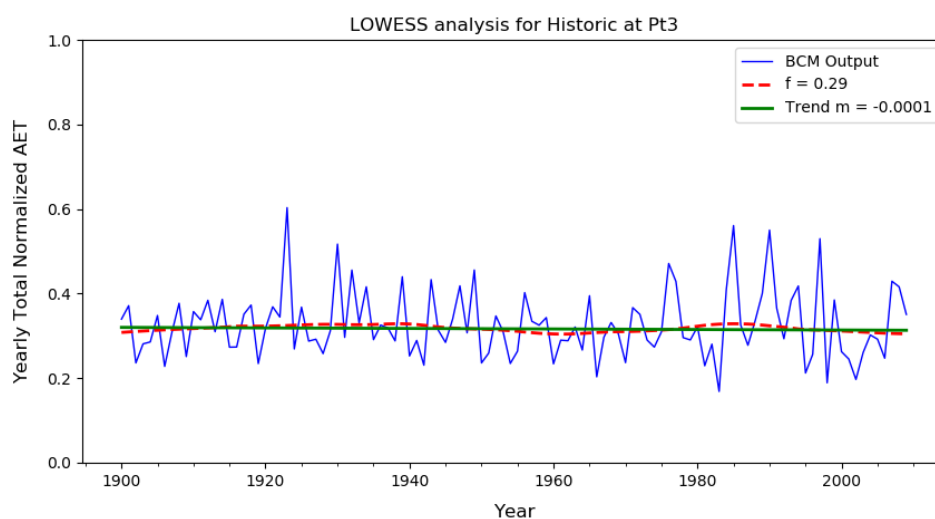


Figure 4.7: BCM output with LOWESS smoothing and trend line at point 3. Even though the slope is statistically different from zero, the magnitude is essentially zero.

GFDL A2

In the projected scenario (for 2011 – 2099), the total yearly precipitation decreases at points 0 – 7. The change in precipitation over time is greatest in the upper elevation areas (0.37 cm/yr at point 0) and decreases with decreasing elevation (0.18 at point 7). A statistically significant trend was not observed at Point 8, which is located near FRS. At the overall basin scale, the average precipitation is 80.8 cm/yr. Similar to the historic scenario, the amount of yearly total precipitation decreases with decreasing elevation (Figure 4.5).

There is no projected trend in yearly total AET at any points except point 1. At this location, there is a slight decrease in AET of 0.074 cm/yr. While this slope is statistically significant, the magnitude is rather small compared to other changes observed. The yearly total snowfall decreases at all point locations. The change in yearly total snowfall over time is greatest in the upper elevation areas (at a rate of 0.53 cm/yr at point 0) and declines with decreasing elevation

Table 4.2: Percent change from historic to projected period at the watershed scale.

Variable	Percent Change from Historic to Projected
Precipitation	-5%
AET	4%
Groundwater Recharge	-12%
April 1st Snowpack	-62%

(at a rate of 0.20 cm/yr at point 8). Snowfall declines more quickly than the trend in precipitation. This indicates that in addition to overall less precipitation, there is a shift in precipitation type from less snow to more rain. Groundwater recharge decreases at points 3, point 4 and point 6 at a rate of 0.25 cm/yr, 0.22 cm/yr, and 0.27 cm/yr respectively. These rates are equivalent to the slope of the Thiel-Sen trend line and represent the rate of change rather than the actual amount. On a watershed scale, the average for yearly total AET and groundwater recharge over the water year are respectively 37.8 cm/yr and 39.0 cm/yr and the average April 1st snowpack is 8.20 cm/yr. Watershed scale changes from the historic to the projected period are shown in Table 4.2

For the normalized output at all locations the normalized yearly total AET increases, while recharge declines. This is the opposite relationship that was observed in the historic scenario. These changes vary somewhat sporadically by location however the smallest changes occur in at the upper elevation points 0 and 6. Additionally, at each point the increase in normalized AET is similar in magnitude to the decline in normalized groundwater recharge. For example, at point 0, normalized AET increase by 0.0002 yr^{-1} and groundwater recharge decreases by 0.0004 yr^{-1} . Similarly, at point 5, normalized AET increase by 0.0013 yr^{-1} and groundwater recharge decreases by 0.0012 yr^{-1} . On a watershed scale, these variations are clearly illustrated in Figure

4.8, where fluctuations in normalized AET and normalized recharge mirror one another. This indicates that, proportionally, the precipitation is increasingly being partitioned into leaving the watershed as AET and at the expense of groundwater recharge under climate change. These changes are observed at each point location and across the watershed as a whole.

Examining correlations between yearly total groundwater recharge and precipitation, AET and snowfall further elucidates these observations. Recharge and precipitation are correlated for both the historic and projected periods at all locations ($r = 0.7 - 0.9$). Additionally, the historic and projected correlation coefficients are similar or identical in magnitude at each individual point. The similarity of correlation between the two periods suggests that the relationship between precipitation and recharge does not change much throughout time. This is observed at

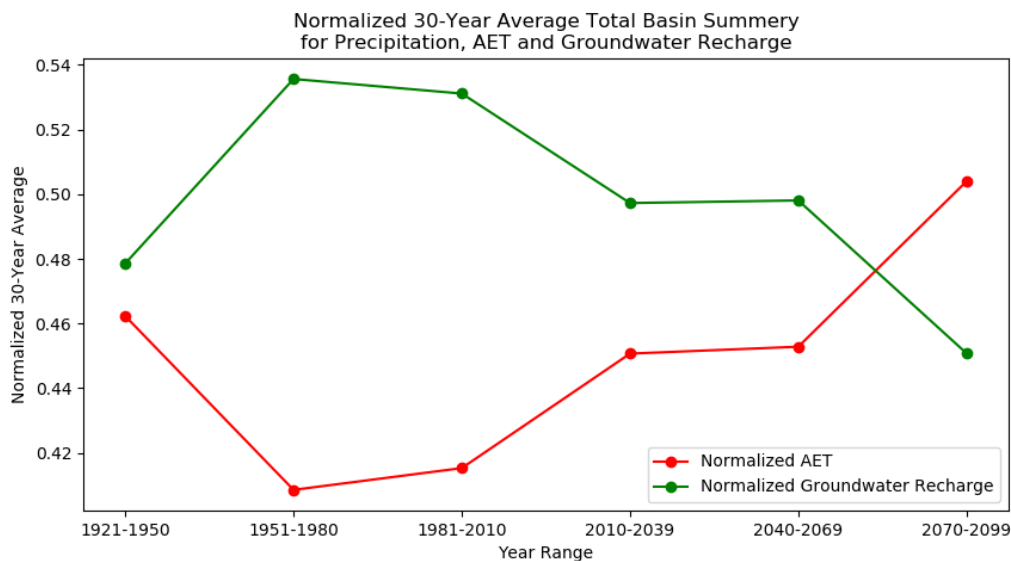


Figure 4.8: Normalized total volume over the watershed for precipitation, AET, groundwater recharge and April 1st snowpack for 30-year averages for historic and projected scenarios.

the basin scale in Figure 4.6 where changes in groundwater recharge generally parallels changes in precipitation.

Total yearly groundwater recharge and total yearly snowfall are also correlated at all points for both the historic and projected scenarios with the exception of point 5 for the projected scenario. For the historic scenario, $r = 0.6 - 0.8$ and for the remaining points in the projected scenario $r = 0.5 - 0.8$. At all locations, the correlation coefficient decreased from the historic to the projected scenario. This suggests that groundwater recharge is more strongly related to snowfall in the historically than under the future climate.

Total yearly groundwater recharge and total yearly AET are not correlated, except weakly so at points 0 and 1 ($r = 0.5$) in the historic scenario. This is observed in the basin scale output in Figure 4.6 where yearly total recharge increases in the historic period and then decreases in the projected, while AET shallowly increases in the historic scenario and appears to somewhat level off in the projected.

Also, of significance is the 30-year average monthly cumulative output. A shift in seasonality occurs for snowfall, AET, and groundwater recharge at all points. For snowfall, the end of the snow season occurs 1-2 months earlier in the year by the end of the century. A similar shift is also observed in both recharge and AET. Historically, most recharge occurs over the late winter months and into early spring with little additional recharge in late spring and summer.

However, the start of this period is shifted 1-2 months earlier in the projected scenario. This is illustrated in Figure 4.9 for snowfall, AET and recharge at point 3 where the timing of snowfall

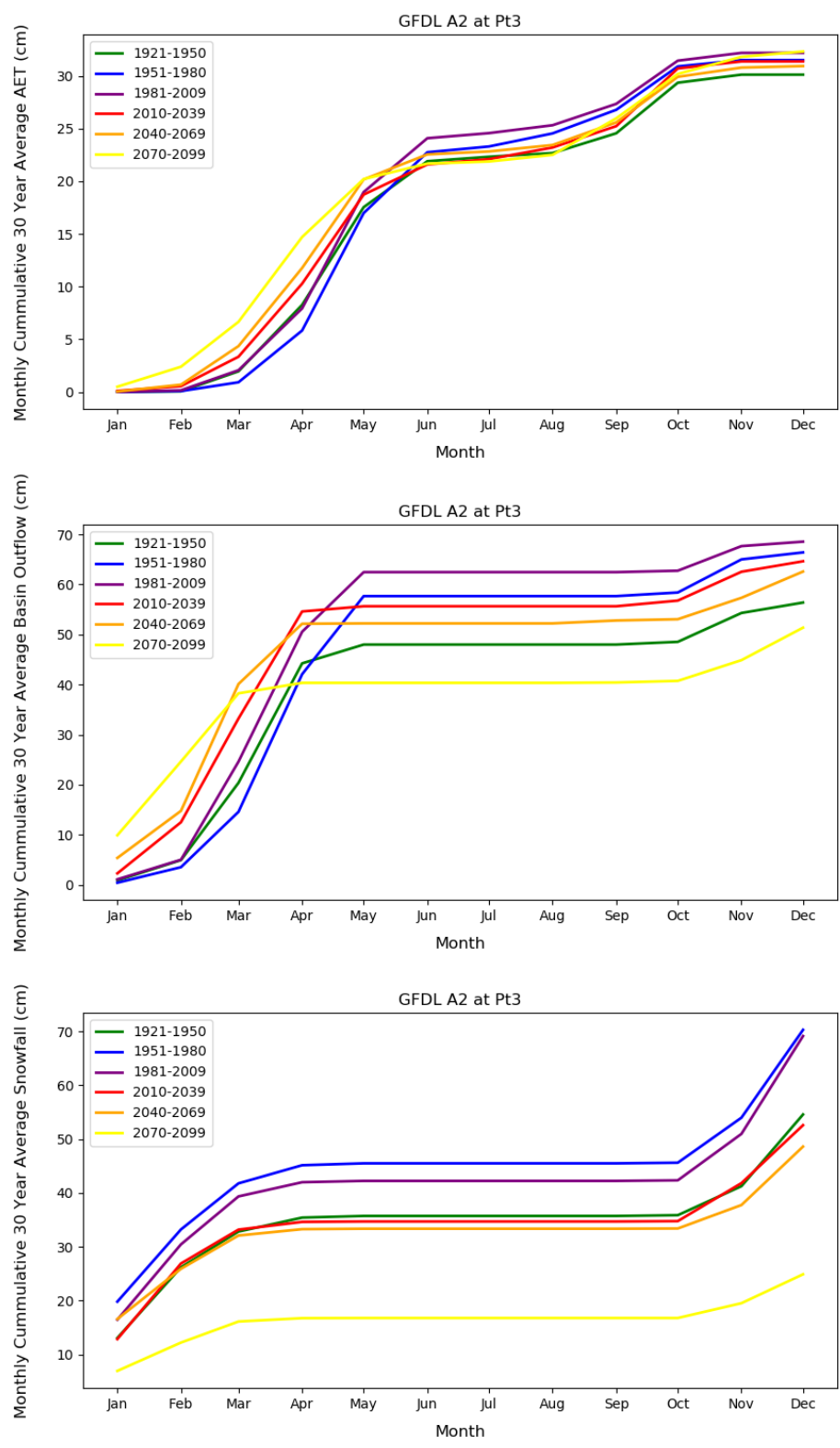


Figure 4.9: Cumulative summary at point 3 for 30-year average AET, groundwater recharge and snowfall. All climate variables shift earlier in the year by 1-2 months by the late projected time period.

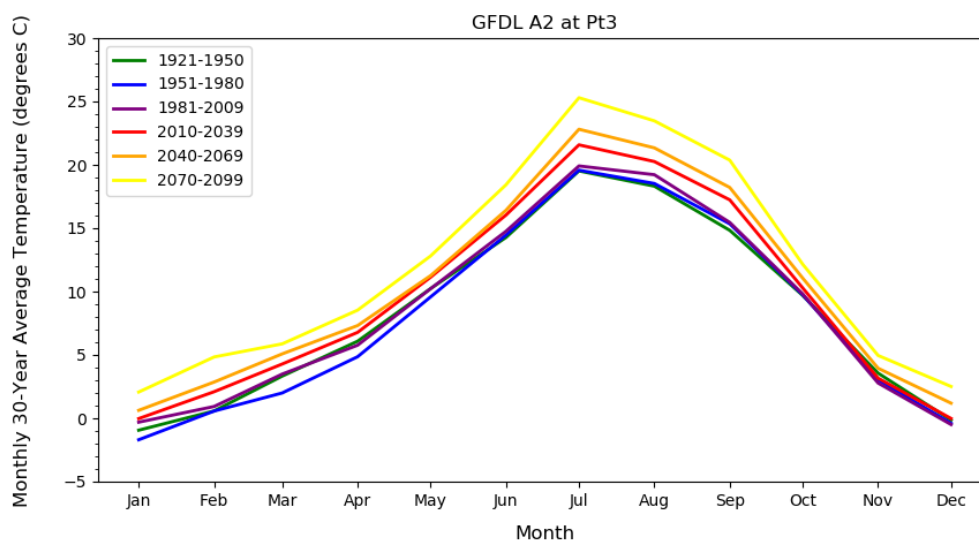


Figure 4.10: Summary at point 3 for 30-year average temperature.

and AET also change to a similar degree. It should also be noted that the changes observed in the timing of AET and groundwater recharge are not coupled with temperature since. While temperature does increase from the historic to project period, the timing of yearly temperature fluctuations remains consistent between the historic and projected periods (Figure 4. 10).

Overall, there is a modest decrease in total yearly precipitation from the historic to the projected scenario. Snowfall decreases more, and more precipitation occurs in the form of rain rather than snow. A greater proportion of the precipitation leaves the system as AET and less becomes recharge with a decrease in average groundwater recharge at the watershed scale.

When precipitation falls as snow, it is held in storage until spring melt. This water is only available for root water uptake once it has been released from storage. Excess water that is not utilized by plants is either held within the soil matrix or infiltrates and becomes recharge. However, as snow decreases, and more precipitation falls as rain, the water is directly and more

immediately available for root water uptake upon infiltration as opposed to being held in storage within the snowpack. Forests throughout the site are largely dominated by lodgepole and sugar pine, and red and white fir, with an understory of bitterbrush manzanita and snowbrush which are active even during the winter months (Modoc National Forest, n.d.). This more continuous root water uptake allows the AET rates to be maintained, despite a decrease in overall precipitation, as water that would be released during spring melt and potentially bypass root uptake is more readily available for plants. This also corresponds to a shift of more AET occurring earlier in the year. The change in timing of AET may also be related to precipitation type as water is more available to plants when precipitation falls as rain instead of snow, leading to more precipitation earlier in the year. It is also possible that the shift in the timing of AET is some function not only of changing precipitation type and amount, but also an overall increase in temperature. Looking at the temperature at which the maximum AET occurs provides insight to whether the shift in timing of AET is influenced by increases in temperature. At points 0 – 7, the temperature at which the maximum AET occurs varies across locations. There is a slight increase in temperature at point 1, 3, 5, and 7 and a slight decrease at point 0, 2, 4, and 6 (Table 4.3, Figure 4.11). Therefore, the temperature at which the maximum AET occurs is relatively consistent when averaged across the locations. This relatively consistent temperature is reflective of the seasonal response of AET shifting earlier in the year, indicating that the overall earlier onset observed in AET is also a function of temperature and this seasonal shift.

At point 8, located at a lower elevation near FRS, the maximum AET occurs at warmer temperatures from the historic to projected time period (Table 4.3, Figure 4.11). The maximum

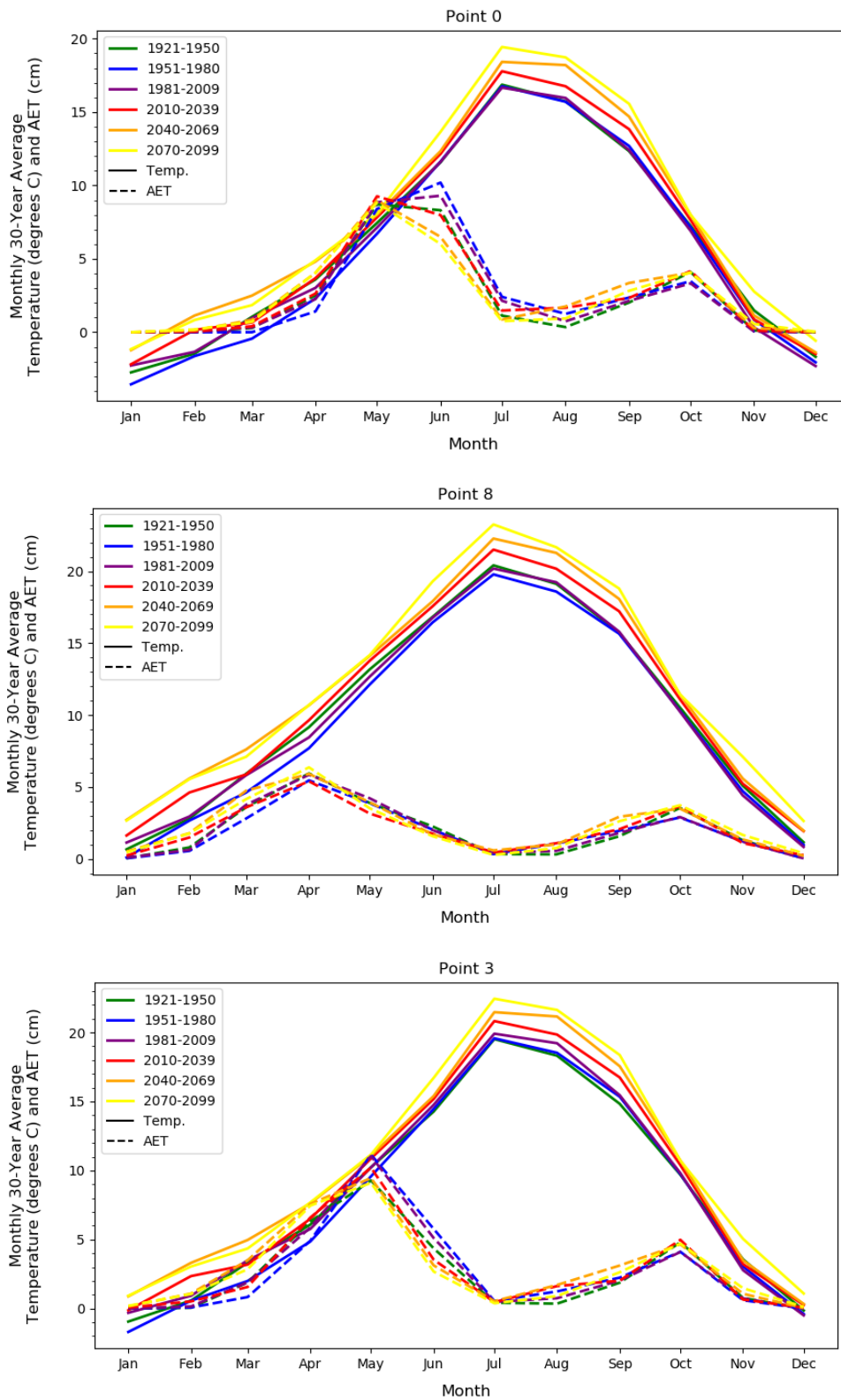


Figure 4.11: Summary comparison of 30-year average temperature and cumulative AET

Point 0	Max AET		Temp at Max AET
	Year	Month	cm
1921-1950	May	8.5	7.5
1951-1980	Jun	10	11.5
1981-2009	Jun	9.5	11.5
2010-2039	May	9.3	8.4
2040-2069	May	9.3	8.4
2070-2099	May	7.5	9.6

Point 1	Max AET		Temp at Max AET
	Year	Month	cm
1921-1950	Jun	15.6	13.5
1951-1980	Jun	15.6	13.5
1981-2009	Jun	15.3	13.5
2010-2039	Jun	16	15
2040-2069	Jun	16	15.5
2070-2099	Jun	14.5	17.5

Point 2	Max AET		Temp at Max AET
	Year	Month	cm
1921-1950	Jun	14.6	13.9
1951-1980	Jun	15.4	14
1981-2009	Jun	15.3	14.3
2010-2039	Jun	14	15.7
2040-2069	Jun	13.5	16.1
2070-2099	May	13.5	12.5

Point 3	Max AET		Temp at Max AET
	Year	Month	cm
1921-1950	May	9.4	10.5
1951-1980	May	11.1	9.5
1981-2009	May	11.1	10.5
2010-2039	May	8.5	11.5
2040-2069	May	8.5	11.5
2070-2099	April	8	8.5

Point 4	Max AET		Temp at Max AET
	Year	Month	cm
1921-1950	May	8.5	10.8
1951-1980	May	10.8	10.3
1981-2009	May	10.3	10.8
2010-2039	May	8	12
2040-2069	May	8	8
2070-2099	April	8	9.3

Point 5	Max AET		Temp at Max AET
	Year	Month	cm
1921-1950	Jun	15.5	15.5
1951-1980	Jun	15	16
1981-2009	Jun	16.5	16
2010-2039	Jun	16.5	17
2040-2069	Jun	16	17.8
2070-2099	May	14	14

Point 6	Max AET		Temp at Max AET
	Year	Month	cm
1921-1950	May	10.5	9.5
1951-1980	May	11.2	9
1981-2009	May	11.2	9.3
2010-2039	May	10.8	10.5
2040-2069	May	10	10.5
2070-2099	April	8.1	8

Point 7	Max AET		Temp at Max AET
	Year	Month	cm
1921-1950	May	13.5	12.5
1951-1980	May	13	11.8
1981-2009	May	13.8	12.3
2010-2039	May	13.8	13.3
2040-2069	May	13.8	13.8
2070-2099	May	12.5	15.3

Point 8	Max AET		Temp. at Max AET
	Year	Month	cm
1921-1950	April	6	9
1951-1980	April	6	7.8
1981-2009	April	5.5	8.5
2010-2039	April	5.8	9.5
2040-2069	April	5.8	10.5
2070-2099	April	5	11.8

Table 4.3: Summary of cumulative 30-year average maximum AET and corresponding temperature at each point location.

AET occurs in April for all time periods, indicating no seasonal shift. This is possibly observed because at point 8 the system has lower precipitation rates (Figure 4.11) and is more water limited. Therefore, even though the temperature increases, there is not enough water to meet the evaporative demand until later in the year.

The earlier onset of AET is key in driving the observed increase in normalized AET and decrease in recharge. For this GCM, the shift in timing appears to be a function of both increasing temperature and a change in precipitation type. Recharge is further impacted by the transition of precipitation type from snow to rain in that water that could have infiltrated and become recharge is now readily available for plant uptake as described above, resulting in less recharge. Furthermore, when precipitation falls as snow, it results in a single infiltration event with spring snowmelt. As the wetting front advances, the water content, and hydraulic conductivity, increase making it easier for the water to infiltrate, as opposed to precipitation falling as rain with multiple separate infiltration events throughout the year. Additionally, since recharge is strongly correlated with precipitation, a decrease in total average recharge at the basin scale likely occurs partially due to the overall decrease in precipitation.

Changes to recharge could have an impact on water users, such as hydropower facilities. PG&E maintains hydropower operations along the Pit River, which is fed by the Fall River, as well as other spring fed rivers and streams. On average, 38% of PG&E's long-term annual hydropower generation originates from volcanic aquifers while during dry years, this value may exceed 50%. Freeman calculated the effect of an increase in recharge of 5% to the Pit River, which resulted in an increase of 354 GWh/yr for the Pit River watershed (Freeman, 2001). Similarly, a decrease in

recharge by 10% can be assumed to decrease potential power production by 708 GWh/yr. This is equivalent to a decrease in hydropower generation from spring fed sources by 30%, or 8% of the total hydropower generation.

Conclusions and Future Work

The amount of average total groundwater recharge at the basin scale decreases from the historic to projected time period from 44.1 cm/yr to 39.0 cm/yr. A similar decreasing trend is observed at three of the selected point locations including points 3, 4 and 6. The decrease in groundwater recharge is highly correlated to a decrease in overall yearly total precipitation. Additionally, a transition in precipitation type from snow to rain affects the timing of when water is available for root water uptake. This leads to a higher proportion of the precipitation going to AET rather than to groundwater recharge, as shown with the normalized output. The change in precipitation type also effects the timing of groundwater recharge, which shifts 1-2 months earlier into the year. When precipitation predominantly falls as rain instead of snow, the water readily infiltrates rather than being stored in the snowpack. This water is then available to become groundwater recharge or AET. It should again be noted that these results were based off of a single GCM and were partially driven by a decrease in overall precipitation specific to GFDL A2. Thus, these conclusions for the FRS system are not definitive, as only a single GCM (GFDL A2) was analyzed.

Future work involves evaluating in detail the sublimation component to further elucidate the remaining portion of the water balance. Additionally, similar analysis will be completed using

other GCMs to examine a range of possible futures. This will provide a more comprehensive look at changes to groundwater recharge and provide a better understanding of the system.

References

- Anderson, E. A. (1976). A point energy and mass balance model of a snow cover. NOAA Technical Report NWS 19. Silver Spring, MD. Retrieved from <http://www.csa.com/partners/viewrecord.php?requester=gs&collection=ENV&recid=7611864%5Chttp://www.agu.org/pubs/crossref/2009/2009JD011949.shtml>
- Cleveland, W. S. (1979). Robust locally weighted regression and smoothing scatterplots. *Journal of the American Statistical Association*, 74(368), 829–836. <https://doi.org/10.1080/01621459.1979.10481038>
- Davisson, M. L., & Rose, T. P. (2014). Recharge and Flow in the Medicine Lake Volcano – Fall River Springs Groundwater Basin, California. *Environmental Forensics*, 66–77. <https://doi.org/10.1080/15275922.2013.873097>
- Flint, A., & Flint, L. (2007). Application of the basin characterization model to estimate in-place recharge and runoff potential in the Basin and Range carbonate-rock aquifer system, White Pine County, Nevada, and adjacent areas in Nevada and Utah. US Geological Survey Scientific Investigations Report 2007-5099.
- Flint, L. E., Flint, A. L., Thorne, J. H., & Boynton, R. (2013). Fine-scale hydrologic modeling for regional landscape applications: The California Basin Characterization Model development and performance. *Ecological Processes*, 2(1), 1–21. <https://doi.org/10.1186/2192-1709-2-25>
- Flint, L. E., & Flint, A. L. (2012). Simulation of Climate Change in San Francisco Bay Basins, California: Case Studies in the Russian River Valley and Santa Cruz Mountains. Scientific Investigations Report. Retrieved from <https://pubs.er.usgs.gov/publication/sir20125132>
- Flint, L., & Flint, A. (2007). Regional Analysis of Ground-Water Recharge. USGS Professional Paper 1703-Ground-water recharge in the Arid and Semiarid Southwestern United States-Chapter B.
- Freeman, G. J. (2001). The Impacts of Current and Past Climate on Pacific Gas & Electric 's 2001 Hydroelectric Outlook (pp. 21–38).
- Freeman, G. J. (2012). Analyzing the impact of climate change on monthly river flows in California's Sierra Nevada and southern Cascade mountain ranges. San Francisco.
- Heller, N. E., Kreidler, J., Ackerly, D. D., Weiss, S. B., Recinos, A., Branciforte, R., ... Micheli, E. (2015). Targeting climate diversity in conservation planning to build resilience to climate change. *Ecosphere*, 6(4), art65. <https://doi.org/10.1890/ES14-00313.1>
- Helsel, D. R., & Hirsch, R. M. (2002). Statistical Methods in Water Resources. In *Hydrologic Analysis and Interpretation* (Vol. 4, pp. 1–524). U.S. Geological Survey. <https://doi.org/10.2307/1269385>

- Lute, A. C., Abatzoglou, J. T., & Hegewisch, K. C. (2015). Projected changes in snowfall extremes and interannual variability of snowfall in the western United States. *Water Resources Research*, 51(2), 960–972. <https://doi.org/10.1002/2014WR016267>
- Lynn, E. (2015). California Climate Science and Data - For Water Resources Management.
- Lynn, E., Schwarz, A., Anderson, J., & Correa, M. (2015). Perspectives and Guidance for Climate Change Analysis. Retrieved from http://www.water.ca.gov/climatechange/docs/2015/Perspectives_Guidance_Climate_Change_Analysis.pdf
- Micheli, E., Flint, L., Flint, A., Weiss, S., & Kennedy, M. (2012). Downscaling future climate projections to the watershed scale: A north San Francisco Bay case study. *San Francisco Estuary and Watershed Science*, 10(4), 32. Retrieved from <https://escholarship.org/uc/item/01n4z228>
- Modoc National Forest. (n.d.). Medicine Lake Highlands. Retrieved from <https://www.fs.usda.gov/detail/modoc/specialplaces/?cid=stelprdb5313077>
- PRIESTLEY, C. H. B., & TAYLOR, R. J. (1972). On the Assessment of Surface Heat Flux and Evaporation Using Large-Scale Parameters. *Monthly Weather Review*. [https://doi.org/10.1175/1520-0493\(1972\)100<0081:OTAOSH>2.3.CO;2](https://doi.org/10.1175/1520-0493(1972)100<0081:OTAOSH>2.3.CO;2)
- Safeeq, M., Shukla, S., Arismendi, I., Grant, G. E., Lewis, S. L., & Nolin, A. (2016). Influence of winter season climate variability on snow-precipitation ratio in the western United States. *International Journal of Climatology*, 36(9), 3175–3190. <https://doi.org/10.1002/joc.4545>
- Thorne, J. H., Boynton, R. M., Flint, L. E., & Flint, A. L. (2015). The magnitude and spatial patterns of historical and future hydrologic change in California's watersheds. *Ecosphere*, 6(2), 1–30. <https://doi.org/10.1890/ES14-00300.1>
- Thorne, J., Boynton, R., Flint, L., Flint, A., & Le, T.-N. (2012). Development and Application of Downscaled Hydroclimatic Predictor Variables for Use in Climate Vulnerability and Assessment Studies. California Energy Commission.

Ch 5 – Conclusions and Future Work

The geochemical analysis in Ch 2 serves to enhance the understanding of the site, as well as provide an idea on the timespan for which the system functions. Analysis of stable isotopes supplements past work and similarly suggests MLV as an area of recharge. The calculated recharge temperature from dissolved noble gases for FRS ranges from 5.1 to 6.8 degrees C. Apparent CFC ages range from 33 to 46 and indicate relatively quick transport times.

Groundwater modeling in Ch 3 provides an estimate of hydrologic parameters and contributes to the conceptual model of the system. Due to the steep hydraulic gradient in the Highlands area, two zones of hydraulic conductivity were defined with an upper zone having a hydraulic conductivity on the order of 10^{-1} m/d and the lower zone equal to 10^2 m/d with an aquifer thickness between 25 – 100m. With a hydraulic timescale of 1-2 years the effective porosity is on the order of 10^{-2} . These bulk properties help to characterize the system.

Analysis of BCM output in Ch 4 elucidates possible changes in the amount of recharge under a shift in precipitation type from snow to rain. The average total groundwater recharge at the basin scale decreases from the historic to projected (GFDL A2) time period from 44.1 cm/yr to 39.0 cm/yr. This decrease corresponds to a decrease in total yearly precipitation, snowfall, and an increase in the proportion of precipitation that becomes AET. The change in precipitation type also affects the timing of groundwater recharge, which shifts 1-2 months earlier into the year.

In order to better understand this complex system, additional analysis of the unsaturated zone thickness and modeling of CFC transport through this zone would provide insight to the apparent age of the groundwater discharge at FRS. A better understanding of the groundwater recharge is necessary for future modeling. Further observation data (measured groundwater head) would be beneficial to improve groundwater modeling, especially along the slope of the Highlands area with the steep hydraulic gradient, as well as in within the lava field itself within the lower zone of hydraulic conductivity. Additionally, a similar analysis performed in Ch 4 will be completed using other GCMs to examine a range of possible futures. This will provide a more comprehensive look at changes to groundwater recharge and provide a better understanding of the system.